Mon. Not. R. Astron. Soc. **000**, 000–000 (2011) Printed 17 February 2022 (MN LATEX style file v2.2)

Formation of galactic nuclei with multiple supermassive black holes at high redshifts

Girish Kulkarni[1,2⋆], Abraham Loeb[1]†
[1]*Institute for Theory & Computation, Harvard University, 60 Garden Street, Cambridge, MA 02138 USA*
[2]*Harish-Chandra Research Institute, Chhatnag Road, Jhunsi, Allahabad 211019 India*

arXiv:1107.0517v1 [astro-ph.CO] 4 Jul 2011

ABSTRACT
We examine the formation of groups of multiple supermassive black holes (SMBHs) in gas-poor galactic nuclei due to the high merger rate of galaxies at high redshifts. We calculate the relative likelihood of binary, triple, and quadruple SMBH systems, by considering the timescales for relevant processes and combining merger trees with N-body simulations for the dynamics of stars and SMBHs in galactic nuclei. Typical haloes today with mass $M_0 \approx 10^{14}$ $\mathrm{M}_\odot$ have an average mass $M_{z=6} = 5 \times 10^{11}$ $\mathrm{M}_\odot$ at $z \sim 6$, while rare haloes with current mass $M_0 \gtrsim 10^{15}$ $\mathrm{M}_\odot$ have an average mass $M_{z=6} = 5 \times 10^{12}$ $\mathrm{M}_\odot$ at that redshift. These cluster-size haloes are expected to host single galaxies at $z \sim 6$. We expect about 30% galaxies within haloes with present-day mass $M_0 \approx 10^{14}$ $\mathrm{M}_\odot$ to contain more than two SMBHs at redshifts $2 \lesssim z \lesssim 6$. For larger present-day haloes, with $M_0 \gtrsim 10^{15}$ $\mathrm{M}_\odot$, this fraction is almost 60%. The existence of multiple SMBHs at high redshifts can potentially explain the mass deficiencies observed in the cores of massive elliptical galaxies, which are up to 5 times the mass of their central BHs. Multiple SMBHs would also lead to an enhanced rate of tidal disruption of stars, modified gravitational wave signals compared to isolated BH binaries, and slingshot ejection of SMBHs from galaxies at high speeds in excess of 2000 km s^{-1}.

Key words: black hole physics – galaxies: nuclei – galaxies:evolution – galaxies:high redshift – galaxies:kinematics and dynamics

1 INTRODUCTION

Most local galaxies host supermassive black holes (SMBHs) at their centres (Richstone et al. 1998; Ferrarese & Ford 2005). The SMBH mass $M_{\rm bh}$ is correlated with properties of the spheroidal nucleus of the host galaxy, such as velocity dispersion (Ferrarese & Merritt 2000; Gebhardt et al. 2000; Ferrarese 2002; Gültekin et al. 2009) and luminosity (Magorrian et al. 1998; McLure & Dunlop 2002; Marconi & Hunt 2003; Gültekin et al. 2009). Detection of bright quasars at redshifts $z \gtrsim 6$ (Fan et al. 2001; Mortlock et al. 2011) suggests that SMBHs with masses as high as $\sim 2 \times 10^9$ $\mathrm{M}_\odot$ already existed at $z \sim 7$. In the standard ΛCDM cosmological model, growth of galaxies is hierarchical and galaxy mergers are expected to be particularly frequent at redshifts $z \sim 6$–20. As galaxies merge, their central SMBHs can grow through coalescence and accretion of gas. It is commonly postulated that SMBHs at lower redshifts grew out of seed black holes (BHs) in the first galaxies (Loeb & Rasio 1994; Eisenstein & Loeb 1995; Kauffmann & Haehnelt 2000; Menou et al. 2001; Bromm & Loeb 2003; Volonteri et al. 2003; Hopkins et al. 2006; Tanaka & Haiman 2009).

Existing merger tree models are based on the assumption that any binary black hole system, which inevitably forms in a galaxy's merger history, coalesces on a short time-scale. However, the evolution of SMBH binaries is a complex open problem and it is unclear if a binary can merge within a Hubble time (Merritt & Milosavljević 2005). One expects that during a merger event of two galaxies, the dynamics of their constituents SMBHs would proceed in three stages (Begelman et al. 1980). In the first stage, the SMBHs sink to the centre of the gravitational potential of the merger remnant by dynamical friction and form a gravitationally bound binary. The newly-formed binary continues to lose energy and angular momentum through its global gravitational interaction with many stars until the separation between the SMBHs reduces to a value at which the dominant mechanism of energy loss is the 3-body interaction between the binary and individual stars. This is the second stage of the binary's evolution, and is known as the 'hard stage.' The precise definition of a hard SMBH binary varies in the literature, but it is commonly assumed that the binary becomes hard when its semi-major axis a reaches a value given by (Yu 2002)

$$a \approx a_h \equiv \frac{Gm}{4\sigma^2} = 2.8 \left(\frac{m}{10^8 \mathrm{M}_\odot} \right) \left(\frac{200 \text{ km s}^{-1}}{\sigma} \right)^2 \text{pc}, \quad (1)$$

where stars in the galactic nucleus are assumed to have a one-dimensional velocity dispersion σ, and m denotes the mass of the lighter SMBH. Finally, once the SMBH separation decreases to a

⋆ Email: girish@hri.res.in
† Email: aloeb@cfa.harvard.edu

© 2011 RAS

small-enough value, gravitational wave emission becomes the dominant mode of energy loss and the SMBHs coalesce rapidly. This is the third stage of the SMBH binary evolution. The value of semi-major axis a at which the coalescence time scale due to gravitational wave emission alone is t is given by (Peters 1964; Loeb 2010)

$$a(t) \equiv a_{\rm gw}(t) = 4.3 \times 10^{-3} \left(\frac{t}{10^5 {\rm yr}}\right)^{1/4} \left(\frac{M}{2 \times 10^8 {\rm M}_\odot}\right)^{3/4} {\rm pc}, \quad (2)$$

where M is the total mass of the binary, and we have considered two SMBHs with mass 10^8 $M_\odot$ each on a circular orbit (with shorter time scale at increasing eccentricity). Gravitational wave emission takes over as the dominant mode of energy loss when $a = a_{\rm gw}(t_h)$, where t_h is the hardening time scale.

Among these three stages of evolution of an SMBH binary, the largest uncertainty in the binary's lifetime originates from the hard stage, which can be the slowest of the three stages since the binary quickly ejects all low angular momentum stars in its vicinity, thus cutting off its supply of stars. This is known as the "final parsec problem" (Milosavljević & Merritt 2003b). For example, Yu (2002) studied coalescence of SMBH binaries in a sample of galaxies observed by Faber et al. (1997) and found that spherical, axisymmetric or weakly triaxial galaxies can all have long-lived binary SMBHs that fail to coalesce. Similarly, Merritt & Milosavljević (2005) found that the time spent by a binary is less than 10^{10} yr only for binaries with very low mass ratios ($\lesssim 10^{-3}$).[1] Furthermore, Merritt & Milosavljević (2005) showed that a binary may not be able to interact with all the stars in its loss cone, thereby increasing the time spent in the hard stage even further; they found that in a nucleus with a singular isothermal sphere stellar density profile, an equal-mass binary will stall at a separation of $a \approx a_h/2.5$, where we have defined a_h in Equation (1). The final separation is expected to be even higher for galaxies with shallower density profiles.

Several ways have been discussed in the literature to efficiently extract energy and angular momentum from a hard SMBH binary and overcome the final parsec problem. An example is the work by Armitage & Natarajan (2002), who suggested that gas can catalyse the coalescence of a hard SMBH binary by serving as an effective sink for the binary's angular momentum. In particular, they found that a binary with a separation of 0.1 pc embedded in a gaseous accretion disk would merge in 10^7 years without significant enhancement in the gas accretion rate. Similarly, Escala et al. (2004, 2005) found that in SPH simulations, clouds of hot gas ($T_{\rm gas} \approx T_{\rm virial}$) can induce decay of orbits of embedded binary point masses due to gravitational drag. A caveat to these studies is that feedback from gas accretion onto the SMBHs can remove the rest of the gas from the merger remnant before the binary coalesces. However, stellar dynamical processes could also accelerate binary coalescence, without gas. For example, Merritt & Poon (2004) considered the effect of chaotic orbits in steep triaxial potentials. They found that stars are supplied to the central black hole at a rate proportional to the fifth power of the stellar velocity dispersion and that the decay rate of a central black hole binary would be enhanced even if only a few percent of the stars are on chaotic orbits, thus solving the final parsec problem. As another example, it was suggested that a third SMBH closely interacting with a hard SMBH binary can reduce the binary separation to a small value either due to the eccentricity oscillations induced in the binary via the Kozai-Lidov mechanism (Blaes et al. 2002) or due to repopulation of the binary's loss cone due to the perturbation in the large-scale potential caused by the third black hole (Hoffman & Loeb 2007). Blaes et al. (2002) found that the merger time scale of an inner circular binary can be shortened by as much as an order of magnitude, and that general relativistic precession does not destroy the Kozai-Lidov effect for hierarchical triples that are compact enough.

In summary, there is substantial uncertainty in the current understanding of the evolution of binary SMBHs. Clearly, if the SMBH binary coalescence time is longer than the typical time between successive major mergers of the galaxy, then more than two SMBHs may exist in the nucleus of a merger remnant. We study this possibility in this paper. We calculate the relative likelihood of binary, triple, and quadruple SMBH systems, by considering the timescales for relevant processes and combining galaxy merger trees with direct-summation N-body simulations for the dynamics of stars and SMBHs in galactic nuclei. An obvious question regarding galactic nuclei with multiple SMBHs is whether such systems can be long-lived. We consider this question here. Finally, systems with multiple SMBHs are likely to be interesting because of observational effects involving their effect on the properties of the host bulge, the enhancement in the rate of tidal disruption of stars, their associated gravitational wave and electromagnetic signals, and the slingshot ejection of SMBHs at high speeds. We study some of these effects.

In §2 we review previous results on galactic nuclei with more than two SMBHs. We present simple analytical arguments regarding the formation and evolution of such systems in §3 and 4. Details about our numerical simulations are described in §5, with their results shown in §6. We consider the observational signatures of our findings in §7. Finally, we discuss and summarise our primary findings in §8.

2 PREVIOUS WORK

Galactic nuclei with multiple SMBHs were first studied by Saslaw et al. (1974), who computed orbits of three and four SMBH systems by sampling the parameter space of the problem. They showed that if an infalling SMBH is lighter than the components of the pre-existing binary, then the most probable outcome is a slingshot ejection in which the infalling SMBH escapes at a velocity that is about a third of the orbital velocity of the binary. Valtonen (1976) further showed that the ejection velocity can be significantly enhanced if drag forces due to gravitational radiation are accounted for in the three-body dynamics. The formation of systems with three or four SMBHs in a hierarchical merger of smooth galactic potentials was first studied by Mikkola & Valtonen (1990) and Valtonen et al. (1994) with the objective of understanding the structure of extragalactic radio sources. This line of work was extended to binary-binary scattering of SMBHs by Heinämäki (2001), and by Hoffman & Loeb (2007), who studied repeated triple interactions in galactic nuclei. Both of these studies used cosmologically consistent initial conditions based on the extended Press-Schechter theory. Systems with a larger number of black holes were studied by Hut & Rees (1992) and Xu & Ostriker (1994) using simple analytical models and numerical calculations of massive particles in smooth galactic potentials. Xu & Ostriker (1994) concluded that the most-likely outcome in these cases is one in which most black holes are ejected and the galactic center is left with zero, or one,

[1] However, for such low mass ratios the time taken by the lighter black hole to reach the galactic nucleus due to dynamical friction is itself expected to exceed the Hubble time.

or two black holes. Finally, full N-body simulations of galactic nuclei with constituent SMBHs were performed for the case of two successive mergers by Makino & Ebisuzaki (1996), Makino (1997), and Iwasawa et al. (2006). Much of this work on SMBHs was based on earlier studies of stellar-mass black holes in globular clusters. Sigurdsson & Hernquist (1993) and Kulkarni et al. (1993) considered the evolution of ~ 100 stellar mass black holes in globular clusters. They concluded that after mass segregation, most of these black holes are ejected out on a short time scale, and the globular cluster is left with none or a few black holes. Mass segregation and associated effects of stellar-mass black holes in a galactic nucleus with a central SMBH was also considered (Miralda-Escudé & Gould 2000; Freitag et al. 2006).

The possible formation of systems with multiple SMBHs due to successive galactic mergers arises naturally in any model describing the hierarchical assembly of galaxies. One approach to modeling SMBH growth involves constructing semi-analytic prescriptions of various characteristic processes, like mergers of galaxies, formation of spheroids, star formation, and gas thermodynamics, coupled with merger trees of dark matter haloes. This approach has been adopted, for example, by Kauffmann & Haehnelt (2000), who also extended it to study possible formation of multiple SMBH systems and implications for the $M_{\rm bh}$–σ relation and density profiles observed in luminous elliptical galaxies (Haehnelt & Kauffmann 2002). Another study by Volonteri et al. (2003) followed merger trees of dark matter haloes and their component SMBHs using Monte Carlo realizations of hierarchical structure formation in the ΛCDM cosmology. They modeled dark matter haloes as singular isothermal spheres and calculated the inspiral of less massive halos in more massive ones by using the Chandrasekhar formula for dynamical friction. Gas accretion to the SMBHs was modeled so as to reproduce the empirical $M_{\rm bh}$–σ relation and the SMBH dynamics was described with analytic prescriptions. In particular, the coalescence time of hard SMBH binaries was calculated from a set of coupled differential equations based on scattering experiments involving the ejection of stellar mass from the loss cone due to the hard SMBH binary and the resultant change in the hardening rate (Quinlan 1996; Merritt 2000). For galaxies that underwent another major merger before their constituent binary SMBH coalesced, a three-body interaction was implemented between the binary and the intruder SMBH. They found that the smallest SMBH was kicked out of the galaxy in 99% of cases, while the binary escapes the galaxy in 8 % of cases. Thus, a significant fraction of galactic nuclei could end up with no SMBHs or offset SMBHs with mass lower than that expected from the $M_{\rm bh}$–σ relation. These results were later extended to incorporate recoil in the SMBH merger remnant due to asymmetric emission of gravitational waves, which mainly affected the $M_{\rm bh}$–σ relation for low-mass haloes by increasing the scatter (Volonteri & Rees 2006; Volonteri 2007; Blecha et al. 2011). Similar semi-analytic models were studied by several other authors to understand the assembly of $z \sim 6$ quasars. However, most of these models ignored the dynamics of multiple SMBHs and assumed prompt coalescence (Haiman & Loeb 1999; Wyithe & Loeb 2003b; Yoo & Miralda-Escudé 2004; Tanaka & Haiman 2009; Shen 2009). As a result, these models did not treat systems with multiple SMBHs.

Lastly, SMBH assembly has also been studied using smooth particle hydrodynamic simulations that attempted to calculate effects of both the gas physics as well as the gravitational dynamics of the large-scale structure within and around galaxies (Hopkins et al. 2006; Sijacki et al. 2007; Li et al. 2007; Hopkins et al. 2007). However, due to poor mass resolution and particle smoothening, these simulations cannot accurately calculate the detailed dynamics of a multiple SMBH systems. Indeed, in most of these studies, black hole coalescence occurs on scales smaller than the smoothening length, which is usually much larger than the expected separation of a hard SMBH binary. As a result, SMBH coalescence is implemented via a subgrid model. Here, we explore for the first time numerical simulations that incorporate the cosmological process of galaxy mergers in the cosmological context along with an accurate treatment of black hole dynamics.

3 FORMATION OF MULTIPLE-SMBH SYSTEMS

Unless they coalesce rapidly, or get kicked out of the host galactic nucleus, we expect multi-SMBH systems to form in galactic nuclei at high redshift due to mergers of galaxies if the typical black hole coalescence timescale is longer than the feeding timescale of new incoming black holes. In this section, we establish a simple theoretical framework for this formation path using analytical estimates of its relevant timescales: *(i)* the major merger time scale of galaxies; *(ii)* the time scale on which a satellite galaxy sinks to the center of a host galaxy so that a close interaction between SMBHs can occur; and *(iii)* the time scale of SMBH coalescence.

3.1 Time scale of incoming SMBHs

Fakhouri et al. (2010) have quantified the average merger rate of dark matter haloes per halo per unit redshift per unit mass ratio for a wide range of halo mass, progenitor mass ratios and redshift. The result is given by a fitting formula derived from the Millennium (Springel et al. 2005) and Millennium-II (Boylan-Kolchin et al. 2009) simulations:

$$\frac{dN}{d\xi dz}(M,\xi,z) = A\left(\frac{M}{10^{12}\mathrm{M}_\odot}\right)^{\alpha} \xi^{\beta} \exp\left[\left(\frac{\xi}{\tilde{\xi}}\right)^{\gamma}\right](1+z)^{\eta}. \quad (3)$$

Here, M is the halo mass at redshift z, and ξ is the mass ratio of progenitors. Mergers with $\xi > 0.3$ are considered major mergers. The best fit values of various parameters are $\alpha = 0.133$, $\beta = -1.995$, $\gamma = 0.263$, $\eta = 0.0993$, $A = 0.0104$ and $\tilde{\xi} = 9.72 \times 10^{-3}$. The average major merger rate per unit time is then given by

$$\frac{dN_m}{dt}(M,z) = \int_{0.3}^{1} d\xi \frac{dN}{d\xi dz}(M,\xi,z)\frac{dz}{dt}. \quad (4)$$

Fakhouri et al. (2010) also provide a fitting formula for average mass growth rate of halos that can be used to calculate the halo mass at redshift z for use in equation (3),

$$\dot{M}(z) = 46.1\,\frac{\mathrm{M}_\odot}{\mathrm{yr}}\,(1+1.1z)\sqrt{\Omega_m(1+z)^3+\Omega_\Lambda}\left(\frac{M}{10^{12}\mathrm{M}_\odot}\right)^{1.1}. \quad (5)$$

Using equation (4) we can now define the time scale of major mergers for a halo as

$$t_{\rm mrg} = \left[\frac{dN_m}{dt}\right]^{-1}. \quad (6)$$

The behavior of this quantity is shown in Figure 1 for three halo masses that discussed here: a Milky Way-like halo that has a mass $M_0 = 10^{12}$ M$_\odot$ at $z = 0$, the typical halo today that has mass $M_0 = 10^{14}$ M$_\odot$ at $z = 0$, and rare haloes with mass $M_0 = 10^{16}$ M$_\odot$ at $z = 0$. (In this paper, M_0 always denotes the halo mass at redshift $z = 0$. We also refer to the average mass of such haloes at other redshifts, by e. g. $M_{z=4}$ and $M_{z=6}$. A halo with $M_0 = 10^{12}$ M$_\odot$ will

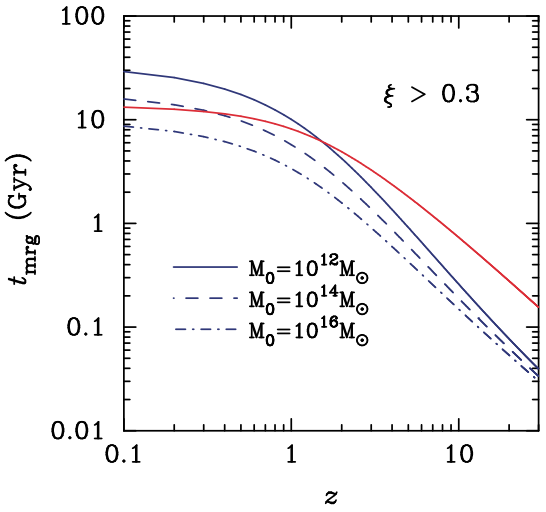


Figure 1. Halo major merger time scale (mass ratio > 0.3), according to equation (6), for haloes with mass $M_0 = 10^{12}$ M$_\odot$ (blue solid line), 10^{14} M$_\odot$ (blue dashed line) and 10^{16} M$_\odot$ (blue dot-dashed line). The Hubble time is shown by the solid red curve. Major mergers are more frequent at higher redshifts. On average, Milky Way-sized haloes are not expected to undergo a major merger for $z \lesssim 1$. Galaxy major merger time scale is always longer than the subsequent dynamical friction time scale.

have $M_{z=6} = 2 \times 10^{10}$ M$_\odot$. A halo with $M_0 = 10^{14}$ M$_\odot$ will have $M_{z=6} = 5 \times 10^{11}$ M$_\odot$. A cluster-size halo, with mass $M_0 = 10^{15}$ M$_\odot$ will have $M_{z=6} = 5 \times 10^{12}$ M$_\odot$ and is expected to hold a single galaxy at that redshift.) This is the time scale at which we expect new (satellite) haloes to enter the halo. As expected, halo mergers are more frequent at higher redshift. At redshift $z \lesssim 1$ the major merger time scale for a Milky Way-like halo is greater than the Hubble time.

After two dark matter haloes have merged, the smaller halo becomes a satellite halo within the virial radius of the host halo. It then takes this satellite a dynamical friction time to sink to the center of the host halo, so that the constituent galaxies can merge. As a result, the timescale for major mergers of galaxies is expected to be different that the time scale for major mergers of dark matter haloes calculated in Equation (6).

The dynamical friction time scale is often estimated using Chandrasekhar's formula (Chandrasekhar 1943; Lacey & Cole 1993; Binney & Tremaine 2008):

$$t_{\rm df} = \frac{f_{\rm df}\Theta_{\rm orb}}{\ln\Lambda}\frac{M_{\rm host}}{M_{\rm sat}}t_{\rm dyn}, \quad (7)$$

where $M_{\rm host}$ and $M_{\rm sat}$ are the masses for the host and satellite haloes respectively, $\ln\Lambda$ is the coulomb logarithm, $\Theta_{\rm orb}$ is a function of the orbital energy and angular momentum of the satellite, $f_{\rm df}$ is an adjustable parameter of order unity and $t_{\rm dyn}$ is the halo dynamical time scale calculated at the virial radius. Equation (7) is valid only in the limit of small satellite mass in an infinite, isotropic and homogeneous collisionless medium. Still, it has been used in the literature even for large satellite masses by modifying the Coulomb logarithm. In recent years, deviations from predictions by equation (7) have been reported in both the $M_{\rm sat} \ll M_{\rm host}$ and $M_{\rm sat} \lesssim M_{\rm host}$ regimes (Taffoni et al. 2003; Monaco et al. 2007; Boylan-Kolchin et al. 2008; Jiang et al. 2008; Wetzel et al. 2009).

To correct the problems associated with Chandrasekhar's formula, several groups have developed full dynamical models of evolution of merging haloes (Taylor & Babul 2001; Gnedin 2003; Taffoni et al. 2003; Zentner et al. 2005). For example, one of the approaches to overcome the limits of Chandrasekhar's formula is the theory of linear response (TLR; Colpi et al. 1999). TLR captures the backreaction of the stellar distribution to the intruding satellite by correlating the instantaneous drag force on it with the drag force at an earlier time via the fluctuation-dissipation theorem. Tidal stripping of a satellite halo is an important ingredient in this formulation. In a singular isothermal sphere with 1D velocity dispersion σ and density profile $\rho(r) = \sigma^2/[2\pi G r^2]$, TLR predicts a sinking time

$$t_{\rm df} = 1.17\frac{r_{\rm cir}^2 V_{\rm cir}}{G M_{\rm sat}\ln\Lambda}\epsilon^{\alpha}, \quad (8)$$

where ϵ is the circularity (defined as the ratio between the angular momentum of the current orbit relative to that of a circular orbit of equal energy), $r_{\rm cir}$ and $V_{\rm cir}$ are the initial radius and velocity of the circular orbit with the same energy of the actual orbit, and $M_{\rm S}$ is the mass of the incoming satellite halo. Numerical simulations suggest a value of 0.4 – 0.5 for the exponent α (van den Bosch et al. 1999; Colpi et al. 1999; Volonteri et al. 2003).

Given the limitations of analytical treatments, we turn to results of numerical simulations to understand the dynamical friction time scale. Using N-body simulations, Boylan-Kolchin et al. (2008) give a fitting formula that accurately predicts the time-scale for an extended satellite to sink from the virial radius of a host halo down to the halo's centre for a wide range of mass ratios and orbits (including a central bulge in each galaxy changes the merging time scale by $\lesssim 10$ %). Their fitting formula is given by

$$\frac{t_{\rm df}}{t_{\rm dyn}} = A\frac{\xi^{-b}}{\ln(1+1/\xi)}\exp\left[c\frac{j}{j_{\rm cir}(E)}\right]\left[\frac{r_{\rm cir}(E)}{r_{\rm vir}}\right]^d, \quad (9)$$

where $A = 0.216$, $b = 1.3$, $c = 1.9$ and $d = 1.0$. Here ξ is the mass ratio $M_{\rm sat}/M_{\rm host}$, j is the specific angular momentum of the satellite halo, and $j_{\rm cir}$ is the specific angular momentum of a circular orbit with the same energy E. This formula is expected to be valid for $0.025 \leqslant \xi \leqslant 1.0$, and for circularities $0.3 \leqslant \eta \equiv j/j_{\rm cir}(E) \leqslant 1.0$. Most likely value of circularity in dark matter simulations is $\eta \approx 0.5$ (Benson 2005; Zentner et al. 2005; Khochfar & Burkert 2006). Lastly, it is valid for range of orbital energy $-0.65 \leqslant r_{\rm cir}(E)/r_{\rm vir} \leqslant 1.0$. This covers the peak value of distribution seen in cosmological N-body simulations. We fix $r_{\rm cir}(E)/r_{\rm vir} = 1.0$ and $\eta = 0.5$, which are the typical values found in simulations.

We can now obtain the instantaneous merger rate of galaxies by combining the halo merger rate and dynamical friction time scale. We closely follow the method of Shen (2009) and write

$$B_{\rm gal}(M,\xi,z) = B[M,\xi,z_e(z,\xi)]\frac{dz_e}{dz}, \quad (10)$$

where $B(M,\xi,z)$ (per unit volume per unit mass per unit redshift per unit mass ratio) is the instantaneous merger rate of halos with mass M, progenitors with mass ratio ξ at redshift z, $B_{\rm gal}$ is the same quantity for galaxies. The redshift $z_e(z,\xi)$ is a function of z and ξ, and is given implicitly by

$$t(z) - t(z_e) = t_{\rm mrg}(\xi, z_e), \quad (11)$$

where $t(z)$ is the cosmic time at redshift z. Shen (2009) finds that dz_e/dz is almost constant at all redshifts for $\xi = 0.1 - 1$ and can be approximated by

$$\frac{dz_e}{dz} \approx 1 + 0.09[\xi^{1.3}\ln(1+1/\xi)]^{-1}, \quad (12)$$

for the fitting formula in equation (9). We assume this form in our

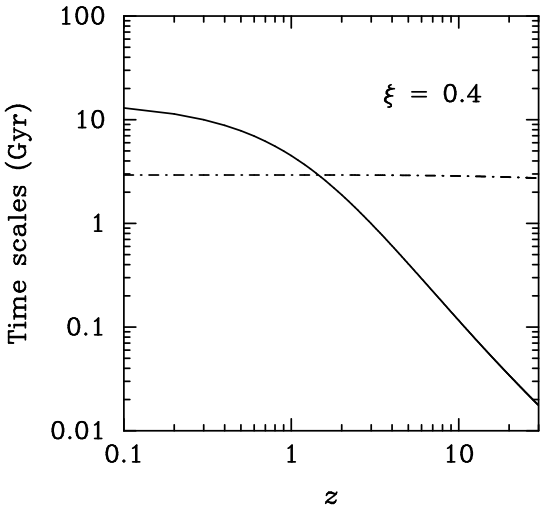


Figure 2. A comparison between the feeding time scale of incoming black holes $t_{\rm in}$ (black solid line; Eq. 13) and the time scale of black hole coalescence $t_{\rm coal}$ (black dot-dashed line; Eq. 23), for a halo mass $M_0 = 10^{12}$ M$_\odot$ and considering only mergers with a mass ratio $\xi = 0.4$. The coalescence time $t_{\rm coal}$ has only a weak dependence on redshift because its dependence on $M_{\rm bh}$ and σ cancel out due to the $M_{\rm bh}$–σ relation. This figure shows that at high redshift new black holes would arrive to the center of a galaxy faster than they could merge via dynamical processes.

calculations. Once we have calculated $B_{\rm gal}(M, \xi, z)$, we normalize it by $n(M, z)$, the abundance of haloes of mass M at redshift z. We use the Sheth-Tormen mass function (Sheth & Tormen 1999) to calculate $n(M, z)$. This gives us the galaxy merger rate *per halo* per unit ξ per unit redshift, which is the galaxy's counterpart of equation (3), and which we denote by $dN_{\rm gal}/dz$. The rate of mergers of galaxies is the rate at which new black holes are added to the host halo's nucleus. Thus, the time scale of incoming black holes is

$$t_{\rm in} = \left[\frac{dN_{\rm gal}}{dz}\frac{dz}{dt}\right]^{-1}. \quad (13)$$

The result is shown by the solid black line in Figure 2 for a mass ratio of $\xi = 0.4$ and a halo that has mass of 10^{12} M$_\odot$ at $z = 0$.

3.2 Binary SMBH coalescence time scale

In order to find whether there is a generic possibility of formation of systems with multiple SMBHs, we compare the time scale on which new black holes are added to the galactic nucleus at a certain redshift with the coalescence time scale of a binary SMBH at that redshift.

As described in §1, the formation and coalescence of a black hole binary is expected to take place in three stages. We define the coalescence time as the time that the binary spends in the second of these stages, that is the time from when the binary separation is $a = a_h$, defined in equation (1), up to when the separation is $a = a_{\rm gr}$ at which point the binary enters the third stage of evolution, and gravitational waves become the dominant mechanism of energy loss. For a hard binary, the dominant channel through which energy is lost is three-body interactions in which stars passing in close proximity to the binary are ejected at a much higher velocity $v_{\rm ej} = [GM_{\rm tot}/a]^{1/2}$, where $M_{\rm tot}$ is the total mass of the binary. The hardening time scale was quantified for a fixed stellar distribution by Quinlan (1996), who found a time scale of

$$t_h(a) \equiv \left|\frac{a}{\dot{a}}\right| = \frac{\sigma}{G\rho a H}, \quad (14)$$

where a is the binary separation, ρ and σ are the density and one-dimensional velocity dispersion of the stellar background, and H is a dimensional parameter whose value was found from scattering experiments to be 16 for a hard, equal-mass binary. In practice, however, the above expression for t_h is valid only during the initial stages of the binary's evolution. As the binary shrinks further, it ejects stellar mass from the central regions and modifies the stellar density ρ that appears in equation (14). This feedback can be quantified using a simple analytical model given by Merritt (2000), in which the binary evolution is described by two coupled equations, the first describing the binary's hardening due to the presence of stars,

$$\frac{d}{dt}\left(\frac{1}{a}\right) = H\frac{G\rho}{\sigma}, \quad (15)$$

and the second describing the change in stellar density due to ejection of mass by the hard SMBH binary,

$$\frac{dM_{\rm ej}}{d\ln(1/a)} = JM_{\rm tot}, \quad (16)$$

where $M_{\rm ej}$ is the ejected mass, and J is another dimensionless parameter that was measured by Quinlan (1996) to be close to unity and nearly independent of a.

By assuming a singular isothermal sphere profile for the stellar density and assuming that the ejected stellar mass causes a constant-density core to form at the center of this profile, Merritt (2000) finds that evolution of the binary separation can be described as

$$\frac{t - t_{\rm init}}{t_0} = \frac{a_h}{a}\left[\ln^2\left(\frac{a_h}{a}\right) - 2\ln\left(\frac{a_h}{a}\right) + 2\left(1 - \frac{a}{a_h}\right),\right] \quad (17)$$

where a_h is as defined in Equation (1), $a(t_{\rm init}) = a_h$, and t_0 is given by

$$t_0 = \frac{9\pi J^2}{H}\left(\frac{M_{\rm tot}}{2m_2}\right)\left(\frac{GM_{\rm tot}}{\sigma^3}\right). \quad (18)$$

This result is found to closely match with the evolution observed in N-body simulation.

On the other hand, the timescale for emission of gravitational waves is given by

$$t_{\rm gr} = \frac{5}{256}\frac{c^5 a^4}{G^3 m_1 m_2 M_{\rm tot}}. \quad (19)$$

As a result, the binary will continue to harden only up to the time when hardening time $t_h = t_{\rm gr}$, after which it will coalesce rapidly due to gravitational wave emission. Using equation (17), it can be shown that this occurs when $a = a_{\rm gr}$ where (Merritt 2000),

$$\frac{a_{\rm gr}}{a_h} \approx A|\ln A|^{0.4}, \quad (20)$$

and

$$A = 9.85\left(\frac{m_1}{m_2}\right)^{0.2}\left(\frac{M_{\rm tot}}{2m_2}\right)^{0.4}\left(\frac{\sigma}{c}\right). \quad (21)$$

Here m_1 and m_2 are masses of the components of the SMBH binary. Finally, we can again use equation (17) to calculate the time it takes for the binary to shrink from $a = a_h$ to $a = a_{\rm gr}$ (Merritt 2000):

$$t_{\rm coal} \approx 8t_0 A^{-1}|\ln A|^{8/5}, \quad (22)$$

which can be simplified as

$$t_{\rm coal} \approx 1.4\times10^{10}{\rm yr}\left(\frac{m_2}{m_1}\right)^{0.2}\left(\frac{M_{\rm tot}}{2m_2}\right)^{0.6}\left(\frac{M_{\rm tot}}{10^9{\rm M}_\odot}\right)\left(\frac{\sigma}{200{\rm km/s}}\right)^{-4}. \quad (23)$$

Clearly, there is a possibility for the formation of multiple-SMBH system if $t_{\rm in} < t_{\rm coal}$. These two time scales are compared in Figure 2 for a halo that has a mass of $M_0 = 10^{12}$ M$_\odot$ at $z = 0$. For simplicity, we have fixed the mass ratio of merging haloes to be $\xi = 0.4$. At each redshift, we calculate $t_{\rm in}$ from equation (13). In order to estimate $t_{\rm coal}$ at a given redshift using equation (23), we first infer the mass of the halo at that redshift from the fitting function for the halo's assembly history from equation (5). We then assume that a galaxy belonging to a satellite halo with mass ratio ξ has merged with this host halo at this redshift.

In order to estimate the mass of black holes in the nuclei of these galaxies, we follow the approach of Hoffman & Loeb (2007) in employing the $M_{\rm bh}$–σ relation. The virial velocity (defined as the circular velocity at virial radius) for a halo of mass M at redshift z is given by

$$v_{\rm vir} = 23.4\left(\frac{M}{10^8h^{-1}M_\odot}\right)^{1/3}\left[\frac{\Omega_m}{\Omega_m^z}\frac{\Delta_c}{18\pi^2}\right]^{1/6}\left(\frac{1+z}{10}\right)^{1/2}{\rm km/s}, \quad (24)$$

where

$$\Omega_m^z = \frac{\Omega_m(1+z)^3}{\Omega_m(1+z)^3+\Omega_\Lambda+\Omega_k(1+z)^2}, \quad (25)$$

and Δ_c is the overdensity of the halo relative to the critical density, given for the ΛCDM cosmology by

$$\Delta_c = 18\pi^2 + 82d - 39d^2, \quad (26)$$

where $d = \Omega_m^z - 1$ (Barkana & Loeb 2001). Further, we equate the halo virial velocity with the circular velocity v_c of its constituent spheroid and obtain the velocity dispersion of the spheroid using the relation (Ferrarese 2002)

$$v_c \approx 314\left[\frac{\sigma}{208{\rm km/s}}\right]^{0.84}{\rm km/s}. \quad (27)$$

This combined with the $M_{\rm bh}$–σ relation (Tremaine et al. 2002)

$$\frac{\sigma}{208{\rm km/s}} \approx \frac{M_{\rm bh}}{1.56\times10^8{\rm M}_\odot}^{1/4.02}, \quad (28)$$

gives

$$\left(\frac{M_{\rm halo}}{10^{12}{\rm M}_\odot}\right) = 8.28\left(\frac{M_{\rm bh}}{10^8{\rm M}_\odot}\right)\left[\frac{\Omega_m}{\Omega_m^z}\frac{\Delta_c}{18\pi^2}\right]^{-1/2}(1+z)^{-3/2}. \quad (29)$$

We obtain the black hole masses in the host and the satellite haloes using equation (29) and use the spheroid velocity dispersion from equation (27) to estimate the coalescence time from equation (23). The result is shown by the dashed line in Figure 2.

At high redshift, early on in the assembly history of a halo, the galaxy merger rate is higher than the SMBH binary coalescence rate and systems with multiple SMBHs can form. Note that the time scale $t_{\rm coal}$ obtained above will change if effect of loss-cone replenishment and gas are taken into account. However, Yu (2002) finds that in realistic spheroidal galaxies, even loss-cone replenishment is insufficient to cause early coalescence.

4 EVOLUTION OF MULTIPLE SMBHS

We have described the literature on systems with more than two SMBHs in §2. If the infalling SMBH is less masssive than either of the components of a pre-existing binary then we expect the ultimate outcome to be ejection of the smaller SMBH and recoil of the binary. Hoffman & Loeb (2007) studied the statistics of close triple SMBH encounters in galactic nuclei by computing a series of three-body orbits with physically motivated initial conditions appropriate for giant elliptical galaxies. Their simulations included a smooth background potential consisting of a stellar bulge and a dark matter halo, and also accounted for the effect of dynamical friction due to stars and dark matter. They found that in most cases the intruder helped the binary SMBH to coalesce via the Kozai-Lidov mechanism and by scattering stars into the binary's loss cone. In this case, the intruder itself was left wandering in the galactic halo, or even kicked out of the galaxy altogether. It was also found that escape of all three black holes is exceedingly rare.

Dynamical evolution of multiple massive black holes in globular clusters has received much attention (Kulkarni et al. 1993; Sigurdsson & Hernquist 1993). From these studies, it is expected that systems with more than two SMBHs will last for about a crossing time.

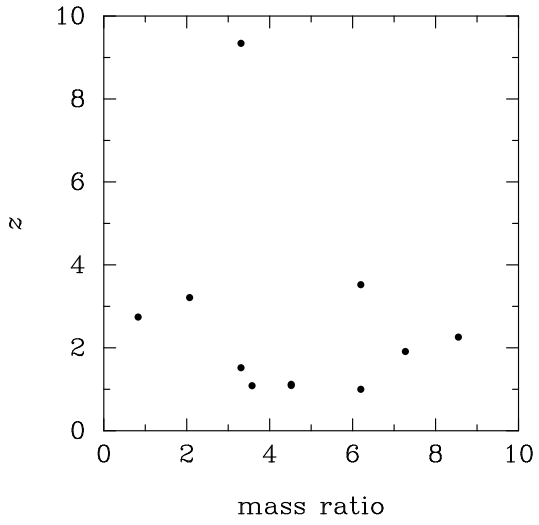


Figure 3. An example merger tree form the Millennium simulation of a halo that has a mass of $M_0 \sim 10^{12}$ M$_\odot$. This plot shows major mergers (mass ratio > 0.1) *in all branches* of the halo's merger tree.

5 SIMULATIONS

In order to accurately calculate the formation and evolution of galactic nuclei with multiple black holes, we perform direct-summation N-body simulations of galactic nuclei merging in a cosmological context. This essentially involves generating physically consistent initial conditions for galactic nuclei with SMBHs at high redshift and evolving them while taking into account the mergers of such nuclei and the resultant close interaction of their SMBHs.

We obtain merger histories of galactic nuclei by extracting merger trees of gravitationally bound subhaloes from the Millennium Simulation Database[2], which stores results of the Millennium Simulation (Springel et al. 2005). The Millennium Simulation is a pure dark matter simulation with a ΛCDM model with 2160^3 particles in a periodic cube 500 h^{-1}Mpc on a side. This corresponds

[2] http://www.mpa-garching.mpg.de/millennium/

Simulation	Mass of halo at $z = 0$ ($M_\odot$)	Max. BH no.	SMBH Coalescences	SMBH Escapes
L1	1.21×10^{14}	4	7	2
L2	1.31×10^{14}	2	1	1
L3	1.31×10^{14}	2	3	2
L4	1.24×10^{14}	2	5	5
L5	1.28×10^{14}	5	8	4
L6	1.31×10^{14}	6	6	0
L7	1.23×10^{14}	3	2	0
L8	1.31×10^{14}	2	3	1

Table 1. Summary of simulations and results for haloes that have a mass of $M_0 \sim 10^{14}$ $M_\odot$. The maximum BH number denotes the number of black holes in the biggest BH group found in a simulation. The last two columns show number of BH coalescences and escapes in the simulation. A halo with $M_0 = 10^{14}$ $M_\odot$ has average mass $M_{z=6} = 5 \times 10^{11}$ $M_\odot$.

Simulation	Mass of halo at $z = 0$ ($M_\odot$)	Max. BH no.	SMBH Coalescences	SMBH Escapes
H1	1.25×10^{15}	6	4	3
H2	1.65×10^{15}	2	1	1
H3	1.81×10^{15}	3	2	0
H4	1.24×10^{15}	5	6	3
H5	1.37×10^{15}	3	7	1
H6	1.40×10^{15}	4	3	0
H7	1.41×10^{15}	6	9	1
H8	1.45×10^{15}	3	4	1
H9	1.46×10^{15}	2	2	0
H10	1.48×10^{15}	4	7	1
H11	1.54×10^{15}	2	1	1
H12	1.59×10^{15}	5	10	1
H13	1.66×10^{15}	8	15	4
H14	1.71×10^{15}	4	3	0
H15	1.81×10^{15}	4	20	7
H16	1.86×10^{15}	3	7	4
H17	4.04×10^{15}	8	11	2

Table 2. Summary of simulation runs with haloes that have mass $M_0 \gtrsim 10^{15}$ $M_\odot$ at $z = 0$. Various columns are same as Table 1. A halo with $M_0 = 10^{15}$ $M_\odot$ has average mass $M_{z=6} = 5 \times 10^{12}$ $M_\odot$.

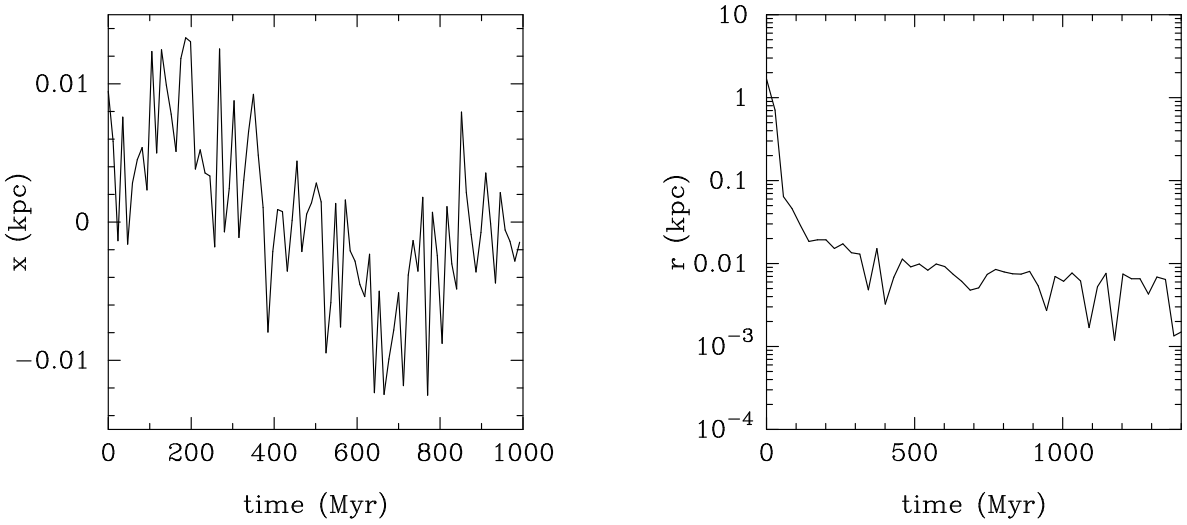


Figure 4. Evolution of single and binary SMBHs in our simulations. (a) The left hand panel shows evolution of the x-component of the position of a 9.95×10^5 $M_\odot$ back hole near the centre of a Hernquist bulge of mass 5.41×10^7 $M_\odot$ and scale length of 0.2 kpc. The particle mass is 5.411×10^3 $M_\odot$. The secular motion is due to that of the cusp. (b) The right hand panel shows evolution of the separation between SMBHs in a binary with initial separation 2 kpc and eccentricity 0.5. The black hole masses were 8.65×10^4 $M_\odot$ and the binary evolved near the center of a Hernquist halo with mass 5.41×10^7 $M_\odot$ and scale length of 10.0 kpc. The particle mass is 5.411×10^3 $M_\odot$.

to a particle mass of 8.6×10^8 h^{-1} M$_\odot$. The output of this simulation is stored in 64 snapshots between $z = 127$ and $z = 0$. Particles in each snapshot are grouped into friends-of-friends (FOF) clusters that are expected to correspond to virialised structures. Each FOF halo contains substructure of gravitationally bound subhaloes that can be related to each other across snapshots as progenitors and descendants. Because a halo can contain multiple galaxies, we expect the subhalo merger tree to reflect the merger history of the galaxies within a halo. Since the goal of this paper is to understand formation and evolution of systems of multiple black holes due to the hierarchical merger history of a galaxy, we extract subhalo merger trees from the Millennium Simulation Database. Each such merger tree typically shows growth of a subhalo via accretion of dark matter particles and via mergers. We process these merger trees to keep only major mergers, which we define to be mergers having mass ratio larger than 0.1. To identify the mass ratio of two subhaloes, we use the masses of the distinct FOF haloes that these subhaloes were a part of before the FOF haloes merged. This is to account for the mass loss of the satellite subhalo due to tidal stripping after it enters the FOF group of the host subhalo, but before the eventual merger of the two subhaloes. (See discussion in §5 of Bundy et al. 2007.) Figure 5 shows the resultant merger history of a Milky Way sized halo. The main reason behind removing minor mergers from our calculation is that for such mergers the dynamical friction time taken by the satellite halo to reach the center of the host halo is longer than the Hubble time. As a result, in such mergers, we do not expect the constituent galactic nuclei of these haloes to interact closely. Since, as we describe below, we model only the spheroidal galactic nuclei in our simulations, we only need to account for mergers in which such nuclei will closely interact. This approach is very similar to that used by Li et al. (2007), with the main difference being our use of direct-summation N-body simulations instead of SPH simulations.

Once we have a galaxy merger tree, we set up the initial conditions of our simulation in the "leaves" of the tree, that is, in haloes that do not have a progenitor, and follow the evolution using an N-body calculation. The initial conditions of our simulation consist of a stellar spheroid with a Hernquist density profile,

$$\rho(r) = \frac{M}{2\pi}\frac{a}{r(r+a)^3}, \tag{30}$$

where M is the total mass of the spheroid and the scale length a is related to the half mass radius $r_{1/2}$ of the spheroid by $a = 0.414 r_{1/2}$. Values for the parameters M and a were obtained from the halo mass as follows (Hoffman & Loeb 2007). We first obtain the black hole mass $M_{\rm bh}$ from the halo mass $M_{\rm halo}$ using Equation (29). We then use the empirical relation between the SMBH mass and the spheroid's virial mass (Magorrian et al. 1998; Marconi & Hunt 2003; Peng et al. 2006) to obtain the latter as

$$M_{\rm sph} = 4.06 \times 10^{10} {\rm M}_\odot \left[\frac{M_{\rm bh}}{10^8 {\rm M}_\odot}\right]^{1.04}. \tag{31}$$

The virial mass of the spheroid is related to its velocity dispersion σ_e and half light radius R_e by

$$M_{\rm sph} = \frac{k R_e \sigma_e^2}{G}. \tag{32}$$

We follow Marconi & Hunt (2003) and set $k = 3$ to get an average ratio of unity between this mass estimate and the dynamically measured masses of galaxies. The velocity dispersion in the above equation is usually measured over either a circular aperture of radius $R_e/8$ or a linear aperture of length R_e. These two methods are in essential agreement, as argued by Tremaine et al. (2002). Assuming a constant mass-to-light ratio for the Hernquist profile, we have $R_e = 1.815a$ and the velocity dispersion at radius $R_e/8$ is given by

$$\sigma_e^2 = \frac{0.104GM}{a}. \tag{33}$$

This lets us obtain the value of the parameter M of the Hernquist profile as $M = 1.765 M_{\rm sph}$. The scale length a is readily obtained as

$$a = \frac{GM_{\rm sph}}{3\kappa_1 \sigma_{\rm bh}^2}, \tag{34}$$

where $\sigma_{\rm bh}$ is obtained using the $M - \sigma$ relation of equation (28). Having obtained a density profile for the bulge, we place a black hole at its center and set the black hole mass to be ten times that obtained from equation (29). This factor of ten is introduced to keep the ratio between the black hole mass and the particle mass high enough (Milosavljević & Merritt 2001; Makino & Ebisuzaki 1996). We confirm that the radius of influence $r_{\rm inf} = Gm_{\rm bh}/\sigma^2$ of this black hole is still much smaller than the a. Velocities of the stars in the spheroid are then generated from the unique, isotropic velocity distribution that corresponds to the gravitational potential of the density profile in Equation (30) and the SMBH (Tremaine et al. 2002). These initial conditions are then scaled to standard N-body units of $G = 1$, $M = 1$ and $E = -0.25$, where M is the total mass of the system and E is its total energy (Heggie & Mathieu 1986; Aarseth 2003). In these units, in virial equilibrium, the mean square velocity $\langle v^2 \rangle = 1/2$ and the system's crossing time is $t_{\rm cr} = 2\sqrt{2}$, independent of the number of particles. The conversion factors from physical units to these N-body units can be easily obtained via dimensional analysis.

Note that we ignore presence of gas in this set-up. Simulations of binary BHs in gaseous environment have not reached sufficient resolution to establish the role played by gas in evolution of SMBHs in galactic nuclei (Merritt & Milosavljević 2005; Colpi & Dotti 2009). Moreover, we expect that at high redshifts, quasar activity triggered by galaxy mergers could efficiently drive gas away from the shallow potential wells of the galaxies.

To perform the actual dynamical evolution of this system, we use the direct-summation code NBODY6 written by Sverre Aarseth (Aarseth 1999, 2003). This code has been well-tested for various applications since around 1992. Its purpose is to perform an exact integration, without particle softening, of a large number of particles. It integrates equations of motion of individual particles using a fourth-order Hermite method with block time steps (Makino & Aarseth 1992). This integrator is coupled with the Ahmed-Cohen neighbour scheme (Ahmad & Cohen 1973), which selects a subset of neighbours of a particle whose forces on it are calculated at a higher time resolution that other, more distant, particles. This scheme reduces the computational cost from $O(N^2)$ to about $O(N^{1.6})$. Close two-body encounters are treated using the Kustaanheimo-Stiefel (KS) regularization method that eliminates the $r = 0$ singularity in Newtonian gravity by using a coordinate transformation. Triples, quadruples and compact subsystems of up to six particles (called "chains") are treated using the chain regularization method (Mikkola & Aarseth 1990). Details of the various algorithms in this code and their implementation are given by Aarseth (2003). In all simulations reported in this paper, the time-step parameter for irregular force polynomial, η_I, and the time-step parameter for regular force polynomial, η_R are set to 0.02. The energy tolerance is set to $Q_E = 4 \times 10^{-5}$ and the regularized time-step parameter is set to $\eta_U = 0.2$.

We check the stability of our initial conditions by evolving standalone realizations of the Hernquist bulge with a central BH and then traverse the merger tree of a given halo using NBODY6, starting from the initial conditions as described above. We scale the physical time between two successive nodes of the tree to N-body units and run NBODY6 for that duration. If a merger happens at a certain node, we place the two galactic nuclei at a distance of 2 kpc apart and evolve in an head-on approach. Although such head-on mergers would be unlikely, we choose it to reduce the computational time while still retaining some realism. When two galaxies, that are in equilibrium separately, merge we expect some transient response in the resulting dynamics. However, as discussed by Milosavljević & Merritt (2001), any such effects in the dynamics of the central regions of the merger remnant of these galaxies are essentially negligible.

Under these conditions, the component black holes approach after a merger event and the remnant galactic nucleus is left with two black holes, which gradually harden due to dynamical friction and three-body interactions with stars in their vicinity. Black hole coalescence is implemented in our simulation by monitoring the separation of hard black hole binaries. Once members of a SMBH binary get closer than a fixed distance $d_{\rm crit}$, we replace them with a single black hole with mass equal to the sum of the masses of component black holes. In all the runs reported in this paper, we set $d_{\rm crit} = 0.1$ pc. Note that this is the only mechanism in which black holes grow in our simulations. Thus, the initial SMBH masses are set according to the $M - \sigma$ relation, but the later growth of these SMBHs occurs only via coalescence.

Recoil due to anisotropic emission of gravitational waves is a natural consequence of asymmetric merger of black holes, either due to unequal masses or due to unequal spins (Peres 1962; Bekenstein 1973). Until recently, it was unclear whether this recoil is large enough to be astrophysicaly relevant. However, recent results from numerical relativity have revealed the resultant kick velocities in a variety of merger configurations (Pretorius 2005; Baker et al. 2006). When the black hole spins are aligned with each other and with the orbital spin, these simulations find revoil velocity of $v_{\rm recoil} \lesssim 200$ km s^{-1} (Baker et al. 2006; González et al. 2007; Herrmann et al. 2007; Lousto & Zlochower 2009). In the absence of spins, this recoil velocity is only a function of the ratio of black hole masses. For random orientations of spins, recoil velocities as high as 2000 km s^{-1} have been obtained (Campanelli et al. 2007a,b). Bogdanović et al. (2007) argue that a circumbinary gas disk can align the binary spins with the orbital axis thereby reducing $v_{\rm recoil}$ to about 200 km s^{-1}. In our simulations we assume a constant kick velocity of 200 km s^{-1}, which we impart to the remnant of every unequal-mass binary SMBH coalescence.

We follow the approach of Makino & Aarseth (1992) and keep the particle number fixed at $N = 10^4$ throughout the simulation. Thus, at every merger, we combine particles in each merging galactic nucleus and double the particle mass. This lets us keep the particle number high throughout the merger tree of the halo. The ratio of black hole mass to the stellar mass is typically a few hundred, which is also roughly the ratio of the spheroid's total mass to the black hole's mass. These values are comparable to other simulations of this kind (Makino & Ebisuzaki 1996; Milosavljević & Merritt 2001).

In summary, the unique features of our simulations are: *(i)* kinematically consistent initial conditions with black holes; *(ii)* calculation of mergers of galactic nuclei in a cosmological setting using merger trees extracted from cosmological N-body simulations; *(iii)* calculation of merger of galactic nuclei resulting in a formation of SMBH binaries starting from the results of each nucleus having evolved in isolation; and *(iv)* accurate calculation of SMBH-star and SMBH-SMBH dynamics throughout the assembly history of a galactic nucleus and its constituent SMBH with the effect of gravitational wave recoil taken into account.

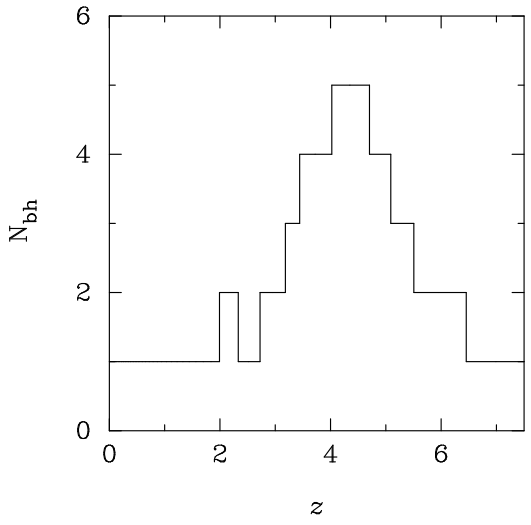


Figure 5. Number of black holes as a function of redshift in a simulation with $M_0 = 1.29 \times 10^{14}$ M$_\odot$.

6 RESULTS

We perform some basic checks on our code, such as ensuring energy conservation and stable evolution of equilibrium systems. In all of our runs, the relative error in the total energy is maintained at $|\Delta E/E| < 4 \times 10^{-5}$. The treatment of BH-BH and BH-star interaction is handled by the original NBODY6 code, and is expected to be accurate. One caveat here is that the neighbour criterion in NBODY6 for regularization of close particles is based on inter-particle distance. As a result, while evolving a set of particles in the vicinity of a massive BH, the code either selects a large number of particles for chain regularization, or selects every close pair of particles for two-body regularization. This usually slows down the code. Indeed, in three of our runs the code run time exceeded practical constraints because of this effect. These three runs are excluded from the results presented below.

6.1 Dynamics of single and binary SMBHs

In a stellar environment, a single SMBH exhibits a random fluctuating motion arising due to discrete interactions with individual stars. As a result, the effect of the stellar environment on the SMBH can be decomposed into two distinct components: (1) a smooth component arising due to the large scale distribution of the whole system, and (2) a stochastic fluctuating part coming form the interation with individual stars (Chatterjee et al. 2002). This random motion is illustrated in the left hand panel of Figure 5, which shows evolution of the x-component of the position of a 9.95×10^5 M$_\odot$ back hole near the centre of a Hernquist bulge of mass 5.41×10^7 M$_\odot$ and scale length of 0.2 kpc. The particle mass is 5.411×10^3 M$_\odot$. As expected, the SMBH wanders around due to stochastic interactions with the stars in its vicinity. The mean square amplitude of these fluctuations

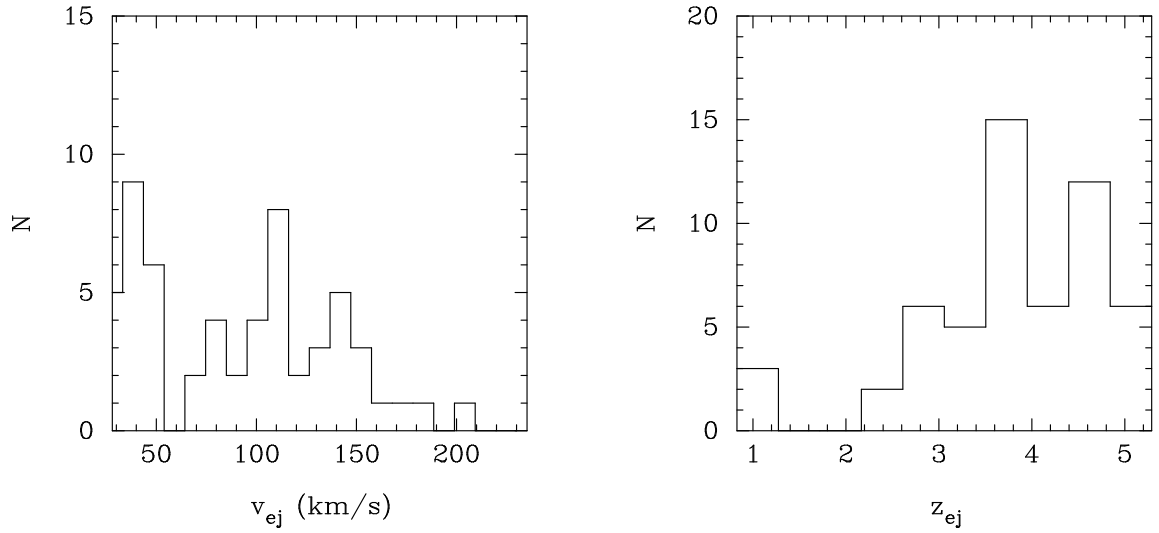


Figure 6. Histograms of ejection velocities of BHs. Left: Velocities of ejected black holes in all of our high mass runs. Note that this does not include ejected black holes with the highest velocities (> 2000 km s^{-1}). Right: number of ejections as a function of redshift in our high mass runs.

is expected to be (Chatterjee et al. 2002; Milosavljević & Merritt 2003a)

$$\langle x^2 \rangle \approx \frac{m_*}{m_{\rm BH}} r_{\rm core}^2, \tag{35}$$

where $r_{\rm core}$ is the radius within which the stellar distribution flattens out. The Hernquist distribution that we have used here does not have a well-defined core, since the density keeps rising as r^{-1} near the origin. Milosavljević & Merritt (2003a) argue that the effective core radius for such distribution can be taken as the radius of influence of the black hole. The resultant mean square value of fluctuations is somewhat smaller that that for Figure 5 by roughly a factor of 2 as is known to happen in N-body simulations (Quinlan & Hernquist 1997; Milosavljević & Merritt 2003a).

As described in §1, the evolution of a binary black hole in a gas-poor galaxy takes place in three stages. Right hand panel of Figure 5 shows evolution of the separation between SMBHs in a binary with initial separation 2 kpc and eccentricity 0.5 in our code. The black hole masses were 8.65×10^4 $M_\odot$ and the binary evolved near the center of a Hernquist halo with mass 5.41×10^7 $M_\odot$ and scale length of 10.0 kpc. The particle mass is 5.411×10^3 $M_\odot$. In the first stage of evolution, the SMBHs sink to the centre of the galactic nucleus by losing energy via dynamical friction and become bound to each other. This stage ends when the separation between the SMBHs is equal to the radius of influence of the binary (Merritt & Milosavljević 2005). In the second evolutionary stage, the binary loses energy predominantly ejection of nearby stars via three-body interaction. The binary loses energy rapidly in this stage, which continues until $t \approx 200$ Myr for the case depicted in Figure 5. The final stage of the SMBH binary evolution begins when the rapid hardening of the second stage stops. This happens when the binary semi-major axis takes the value given by Equation (1). The binary semi-major axis is related to the separation r by

$$\frac{1}{a} = \frac{2}{r} - \frac{v^2}{\mu}, \tag{36}$$

where v is the relative velocity of the BHs and μ is the reduced mass (Makino & Funato 2004; Berczik et al. 2006; Merritt et al. 2007; Khan et al. 2011). In N-body simulations, the last stage is known to have a dependence on the number of particles N such that the hardening rate decreases with increasing N (Makino & Funato 2004).

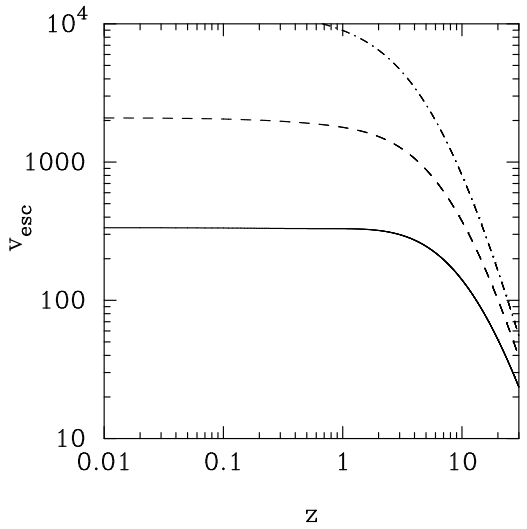


Figure 7. Escape velocities from the bulges of haloes in our three categories of present-day masses of haloes. Solid line: $M_0 \approx 10^{12}$ $M_\odot$, Dashed line: $M_0 \approx 10^{14}$ $M_\odot$, Dot-dashed line: $M_0 \gtrsim 10^{15}$ $M_\odot$. Note that these are average values computed from the fitting functions to the Millennium simulation. Therefore, case by case comparison with our runs is not straightforward.

For real spherical galaxies, the binary separation would stop evolving after this point because the loss cone is empty.

6.2 Evolution of nuclei with multiple SMBHs

We now run the simulation along merger trees of haloes drawn from the Millennium simulation as described in Section 5. These simulations are described in Tables 1 and 2. We randomly select 8 haloes with mass M_0 around 10^{14} $M_\odot$ at $z = 0$. These correspond to the typical haloes ($M \approx M_*$) in the present epoch. We also randomly select 17 haloes whose present-day mass M_0 is in excess of 10^{15} $M_\odot$. These are rare, high mass haloes that are expected to host the redshift 6 SDSS quasars (Li et al. 2007). Additionally, we have also

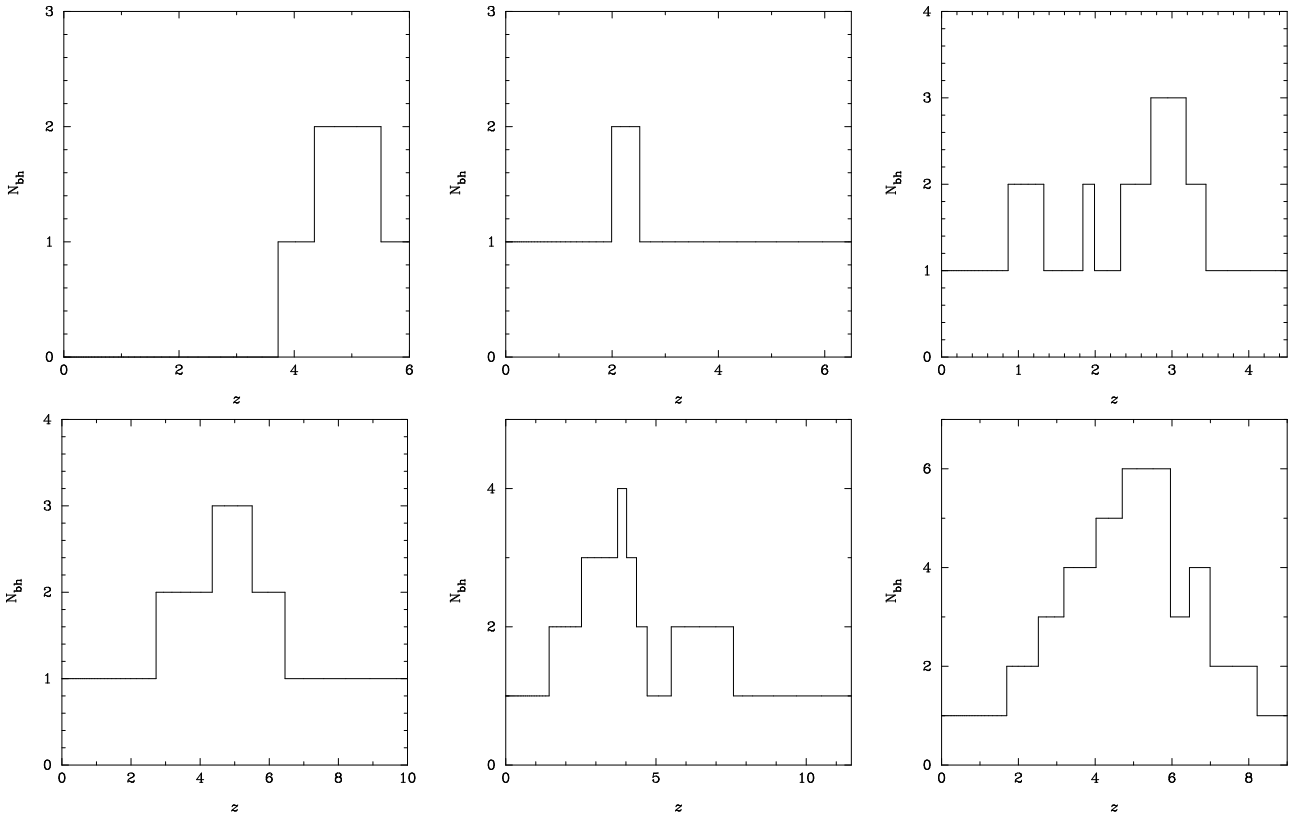


Figure 8. Number of black holes as a function of redshift in a few of our simulation runs.

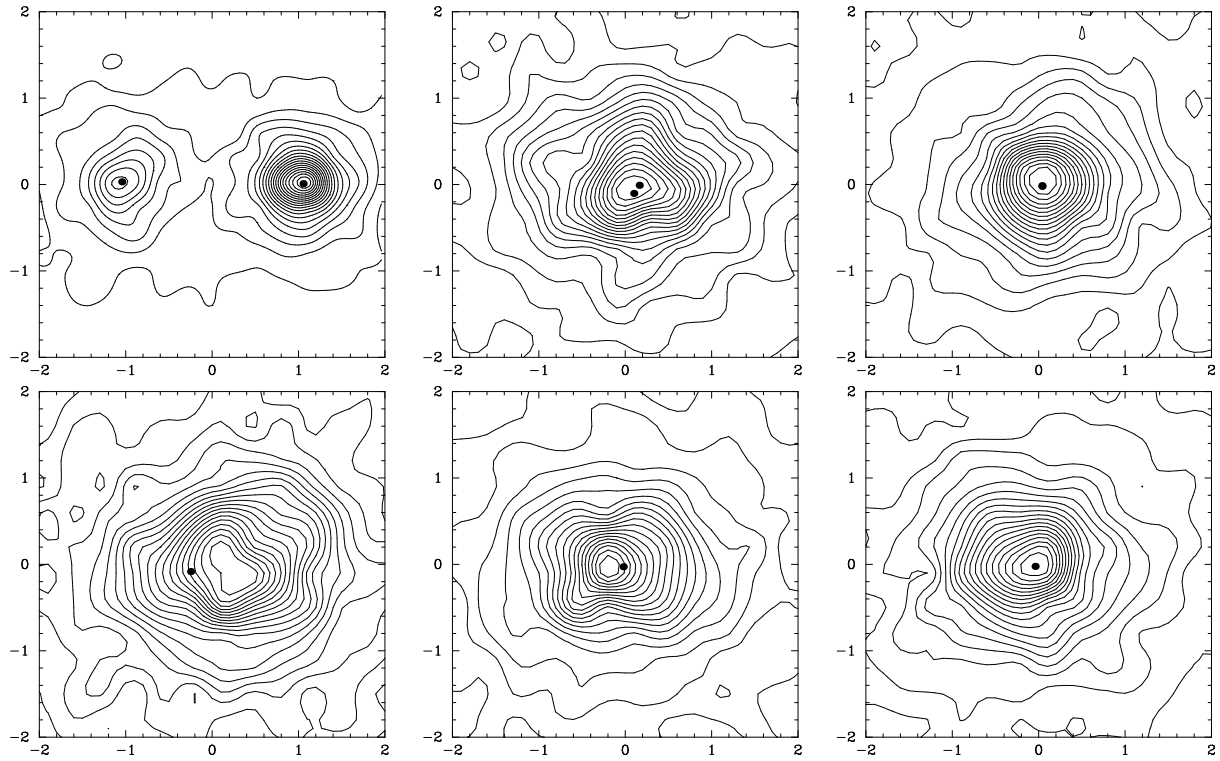


Figure 9. Projected stellar density contours in the presence of a binary in the simulation H5. Each panel is 400 pc on a side. Clockwise from top left to bottom right, the redshifts are z = 10.073, 8.54, 7.27, 6.19, 5.28, and 4.52. The total time span is about 800 Myr. Core-SMBH oscillations are clearly visible.

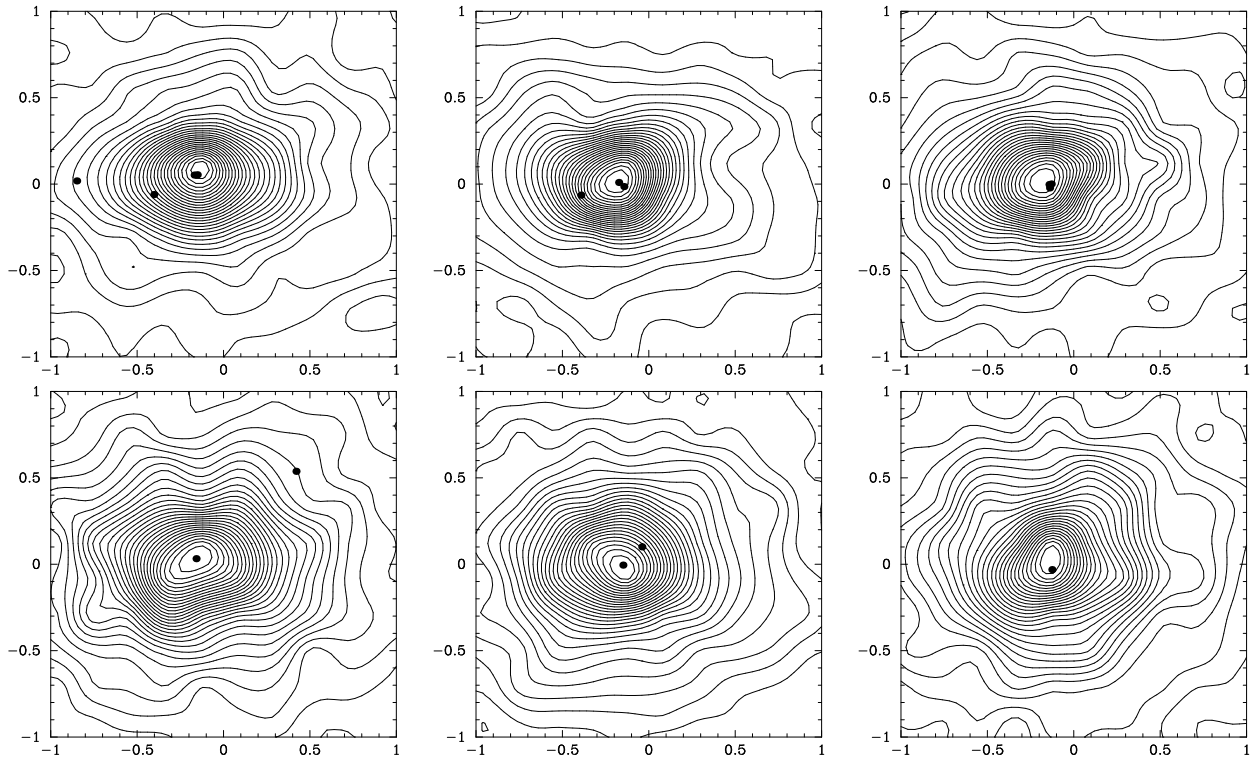


Figure 10. Projected stellar density contours in the presence of multiple BHs in the simulation H4. Each panel is 100 pc on a side. The total time span, clockwise from top left to bottom right, is about 1 Gyr. Most BHs are stripped of their cusps in nuclei with multiple BHs.

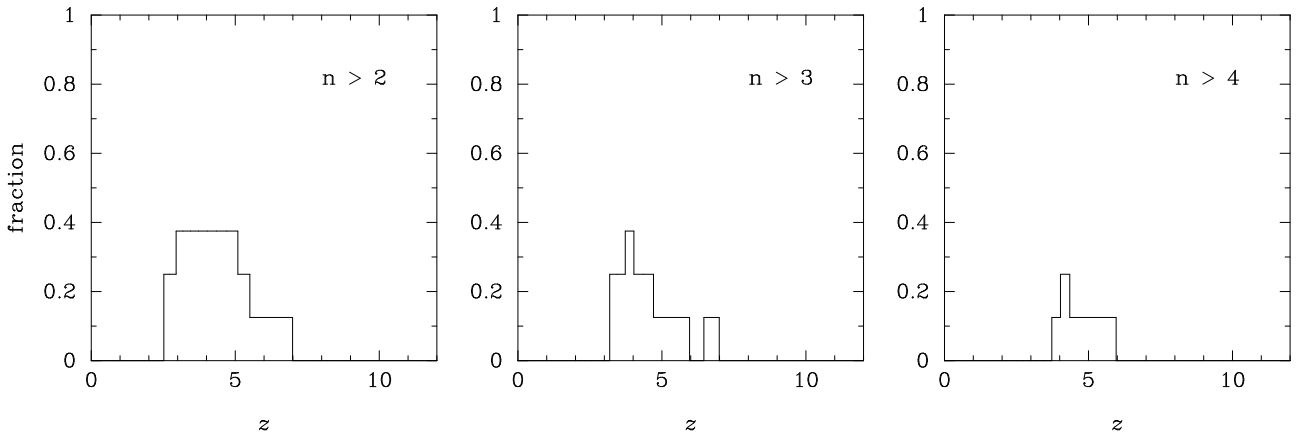


Figure 11. The fraction of runs with multiple SMBHs at different redshift bins for haloes with a mass $M_0 \sim 10^{14}\mathrm{M}_\odot$ at $z = 0$. The results of these runs are summarised in Table 1. The three panels from left to right describe the occurrence of systems with more than 2, 3 and 4 black holes respectively. At each redshift, this number can be interpreted as the likelihood of finding such systems in haloes of mass $M_0 \sim 10^{14}\mathrm{M}_\odot$ at $z = 0$. It is seen that systems with multiple SMBHs are rare at redshift $z \lesssim 2$. Note that a halo with $M_0 = 10^{14}$ M$_\odot$ will have $M_{z=6} = 5 \times 10^{11}$ M$_\odot$.

simulated 11 haloes with present-day mass similar to the Milky Way halo ($M_0 \sim 10^{12}$ M$_\odot$).Using the prescriptions described in the previous section, and using the N-body integrator, these simulations tell us about the effect of multiple mergers of galactic nuclei with SMBHs.

Figure 5 shows results from a typical simulation run, for a halo of mass 1.29×10^{14} M$_\odot$. We plot here the number of BHs in the bulge in the main branch of the galaxy's merger tree at various redshifts. It is seen that the central bulge has more than one SMBH for a wide redshift range ($2 \lesssim z \lesssim 6$; about 2.5 Gyr). For $3 \lesssim z \lesssim 5$ (about 1 Gyr) the bulge holds more than 2 BHs. The maximum number of BHs interacting within the bulge in this simulation is 6. Lastly, the number of BHs reduces to one well before $z = 0$ due to coalescences and ejections. Note that at the highest redshifts ($z \gtrsim 6$) there are no BHs in the central bulge. This is simply an artifact of the limited numerical resolution of the Millennium simulation, because of which the halo merger tree is not resolved at these redshifts. To ensure that this does not affect our results for $z \lesssim 6$, we set up initial conditions at $z \sim 6$ such that the BHs are on the $M - \sigma$ relation, and by using a Hernquist bulge with inner slope

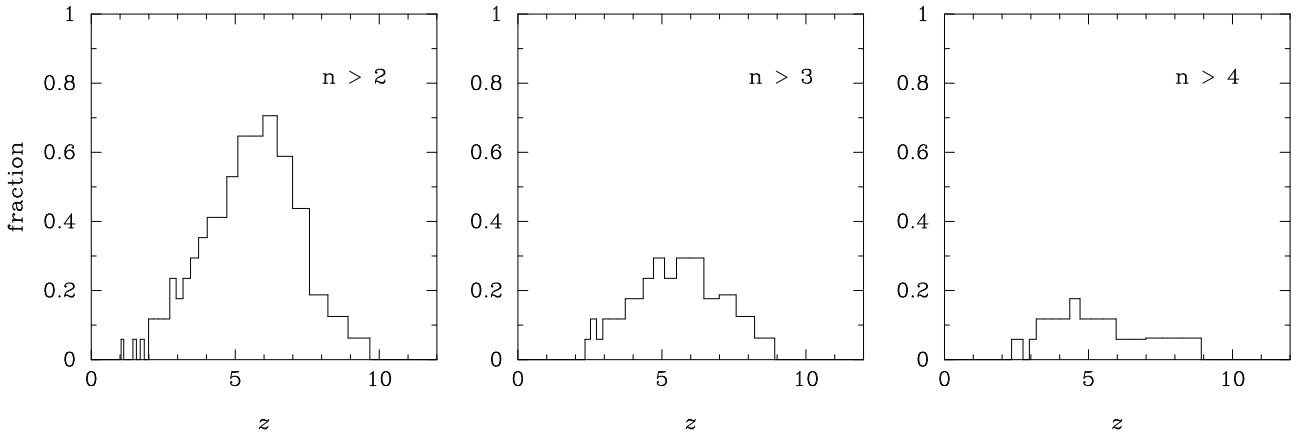


Figure 12. The fraction of runs with multiple SMBHs at different redshift bins for halo masses $M_0 \gtrsim 10^{15}$M$_\odot$ at $z = 0$. The results of these runs are summarised in Table 2. The three panels from left to right describe the occurrence of systems with more than 2, 3 and 4 black holes respectively. At each redshift, this number can be interpreted as the likelihood of finding such systems in haloes of mass $M_0 \gtrsim 10^{15}$M$_\odot$ at $z = 0$. It is seen that systems with multiple SMBHs are rare at redshift $z \lesssim 2$. These results can be compared with those in figure 11. Nuclei with multiple SMBHs are more likely in high mass haloes because of higher merger rate. Note that a halo with $M_0 = 10^{15}$ M$_\odot$ will have $M_{z=6} \sim 10^{12}$ M$_\odot$.

−1. In the absence of gas, the systems with multiple SMBHs form generically, in high mass haloes with frequent of major mergers. It is evident than such systems are usually short-lived and most often these nuclei contain a single SMBH at $z = 0$. Most SMBHs escape into the halo, where they join a population of wandering black holes or escape the halo completely.

Similar results from a few other simulation runs for haloes with mass $M_0 \sim 10^{14}$ M$_\odot$ at $z = 0$ are shown in Figure 8. Most of these runs have features similar to the run described above. Multiple BH systems form generically and last for 2−3 Gyr. Importantly, most of these galaxies end up with a single SMBH in their central bulge. This is in contrast with expectations from some simple arguments in earlier work (Hut & Rees 1992). About 5% of galaxies in our simulations end up with no BHs in their centres at $z = 0$. Tables 1 and 2 summarize these features of all our simulations. The last columns of these tables show the cumulative number of BHs that were ejected out of the galactic nucleus throughout the run either due to recoil associated with emission of gravitational waves or due to many-body interaction between the BHs. We find that for most triple and quadruple SMBH systems in our calculation, gravitational wave recoil is the dominant mechanism for SMBH escape. Many-body interaction between SMBHs was the dominant cause only when the number of black holes was more than four. Consequently, for low-mass galaxies in which the number of BHs is small, almost all escapes were because of gravitational wave recoil. Whereas in our low mass galaxy simulations, larger number of coalescence usually results in large escapers, in the high mass galaxy simulations, coalescence often does not lead to escape. In high mass galaxies, BH-BH interaction is the dominant mechanism behind escaping SMBHs. Figure 6 summarizes this. The right hand panel shows that most ejections happen at high redshifts. Typical ejection velocities are seen in the left hand panel. Ejection velocities are spread out up to 200 km s^{-1}, which is the GW recoil kick in our simulations. Note that this plot does not show kicks with very high velocities, which we describe below.

With the prescription that we have adopted in this paper, we find that SMBH coalescence happens in each one of our simulations. Tables 1 and 2 give the number of BH coalescences occurring in our simulations. Due to the limitation on the particle number, our simulations implement BH coalescence by replacing a bound binary BH by a single BH whose mass is equal to the total mass of the binary. As an example, Figure 9 shows the merger of two bulges beginning from initial conditions at redshift 6.7 in the run H5. In Figure 9, the hardening radius is $a_h = 0.5$ pc at $t_h = 500$ Myr. We find the the BHs remain associated with their host cusps until cusp coalescence. It is known that by increasing the effective mass of the BHs, this increases the rate of coalescence of the BHs by as much as ~ 6 times compared to the dynamical friction time scale. We also see the homology of density structure before and after the merger, as reported previously in the literature (Milosavljević & Merritt 2001). However, one prominent difference from previous works is in the evolution of the density profile in the later stages of the merger. In our simulations, each coalescence event is followed by recoil of the remnant at 200 km s^{-1}, which at high redshift, usually results in the escape of the SMBH from the galaxy. At relatively low redshifts, the recoiled SMBH returns to the nucleus in few hundreds Myr. Because of this recoil, the remnant BH is detached from its cusp immediately. At the recoil speed implemented here, this happens at a much smaller time scale that the local crossing time scale. As a result, the only effect of the remnant on the cusp is due to subsequent core passages.

Usually, most coalescences are assumed to take place due to BH hardening via BH-star encounters. In gas-free systems, this leads to the final parsec problem. In our simulations, we find that in high mass haloes, roughly half of the SMBH coalescences are due to three-body scattering with intruder SMBHs. This is expected, since in spite of higher major merger rate, high mass galaxies in our model are still left with at most two SMBHs at $z = 0$. The dominant mechanism of coalescence is then three body interactions. Figure 8 shows an example of the evolution of a multiple BH system that undergoes three coalescences due to BH-BH dynamics. We find violent oscillations of the cusp-BH system as shown in Figure 9. This has significant impact on the density distribution of the core, and also results in off-centre BHs, which slowly return to the centre of the cusp due to dynamical friction.

About 10% of SMBH ejections in our simulations occur at very high speeds of $\gtrsim$ 2000 km s^{-1}. In haloes with $M_0 \approx 10^{15}$ M$_\odot$ these SMBHs will linger in the outskirts of the halo for 2 – 10

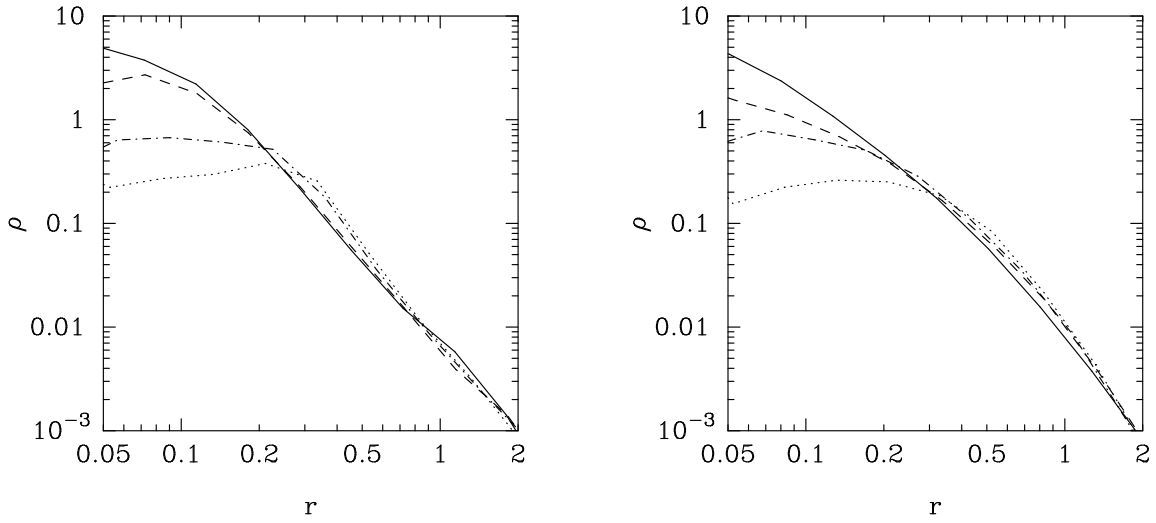


Figure 13. Evolution of density profile for simulations H3 and H5 in N-body units. The solid line is the original Hernquist profile with an inner logarithmic slope of $\gamma \approx -1$. Dashed line shows the profile after one SMBH binary coalescence, dot-dashed line after the second coalesence and the dotted line after the third coalescence. These plots are shown in N-body units to scale out the doubling of the half-mass radius. See text for details.

Gyr as can be seen by comparing with the bulge escape speeds in Figure 7. The SMBHs in the wandering phase that are introduced via this mechanism have markedly different properties than the BHs introduced due to galaxies that have not yet reached the host galaxy's center so as to have a close encounter (Volonteri et al. 2003). The main difference is that our ejected black holes are much more massive than those in the other category. Moreover, the velocity of ejected SMBHs will typically be higher that black holes in the other category, which have already experience significant dynamical friction. Three of the 30 BH ejections in our runs are ejected binaries.

6.3 Likelihood of nuclei with multiple SMBHs at high redshift

From the results of our simulations, we can estimate the likelihood of galactic nuclei with multiple black holes at high redshifts. The histograms in Figures 11 and 12 show fraction of runs with multiple SMBHs at each redshift for haloes with present-day masses of $\sim 10^{14}$ $M_\odot$ and $\sim 10^{15}$ $M_\odot$, respectively. The three panels from left to right describe the occurrence of systems with more than 2, 3 and 4 black holes respectively. At each redshift, this number can be interpreted as the likelihood of occurrence of such systems at that redshift.

Systems with more than 2 SMBHs are generically expected in the central galaxies of haloes with $M_0 \gtrsim 10^{14}$ $M_\odot$ at around $z \gtrsim 3$. On the other hand, few galaxies hold multiple black holes at redshifts $z \lesssim 2$ because the galaxy merger rate is low at these redshifts and the BHs have sufficient time to coalescence. This is consistent with the expectation from our heuristic analysis of Section 3. In other words, multiple black hole systems are numerous at around redshifts of 6, when there are many major mergers in the system. Our numerical simulations show that such systems can exist in sufficiently long-lived configurations of SMBHs separated on pc–kpc scale. Note that these histograms show the likelihood of such systems to be zero at redshifts $z \gtrsim 10$. However, this is simply because the Millennium simulation merger trees do not resolve progenitors at these redshifts. As mentioned before, we have minimized the effect of this shortcoming on our results by requiring that the SMBHs always follow the $M - \sigma$ relation initially.

High mass galaxies ($M_0 \approx 10^{15}$ $M_\odot$) are more likely to have multiple BHs in their nuclei at higher redshift. About 60% of these galaxies have more than 2 BHs between redshifts $z \approx 2$ and 10. This fraction is less than 40% for the low mass galaxies ($M_0 \approx 10^{14}$ $M_\odot$) The likelihood of occurrence of more than 3 and 4 BHs is similar, about 30%, in the two categories of simulation. However, for the high mass galaxies this likelihood is spread out over a wider range in redshift, again due to the higher rate of major mergers.

It is extremely rare for Milky Way-sized galaxies (halo mass $M_0 \approx 10^{12}$ $M_\odot$) to have more than three SMBHs in their nuclei at any moment in their assembly history. Indeed, in our simulations of these galaxies, only one run shows a triple BH system. The main reason behind this is the smaller number of major mergers for these galaxies. Moreover, it is easier for SMBHs to escape the nuclei of predominantly small mass progenitors of these galaxies.

6.4 Effects on the stellar distribution

Most bulges and early-type galaxies have a shallow cusp near their centre. The mass distribution in this region can be described as a power law $\rho \propto r^{-\gamma}$. Most galaxies have slope $0.5 \lesssim \gamma \lesssim 2.0$ (Ferrarese et al. 2006; Merritt & Szell 2006). We expect the constituent SMBH in the bulge to affect the mass distribution within its radius of influence. Only two galaxies, the Milky Way (Genzel et al. 2003) and M32 (Lauer et al. 1998), have been resolved at these small distances. Both these galaxies have $\gamma \approx 1.5$ in their innermost regions.

It is commonly postulated that cores can form in elliptical galaxies and spiral bulges due to mass ejection by a hard binary SMBH (e.g. Milosavljević & Merritt 2001). However, the mass ejected by a hard binary is of the order of the black hole mass. In other words, the mass deficiency $M_{\rm def}$, which is the difference between the mass of the initial and final density distribution in a region around the centre, is roughly $M_{\rm bh}$, the total mass of the SMBH binary. The possibility of enhanced mass deficit because of repeated core passages of recoiled black holes (Gualandris & Merritt 2008) and due to repeated mergers (Merritt 2006) has been consid-

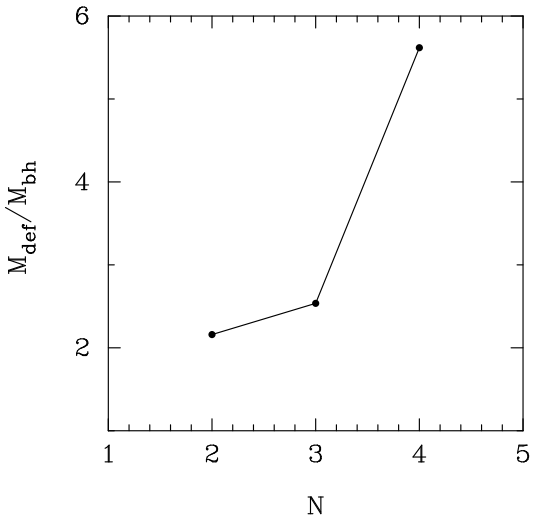


Figure 14. Mass deficiency versus number of coalescences averaged over ten simulation runs. The presence of multiple SMBHs generally leads to larger mass deficiency compared to a single hard SMBH binary.

ered in the literature. Our simulations allow us to understand the effect of both of these factors in addition to the mass deficit produced by simultaneous presence of multiple SMBH in the galactic bulge.

Figure 6.2 shows the cusp evolution in two of our simulations, each of which has four SMBHs and three coalescences. Density profiles after each coalescence is shown. Strong core formation is clearly seen. We calculate $M_{\rm def}/M_{\rm bh}$ for ten such runs and show the average result in Figure. Clearly $M_{\rm def}/M_{\rm bh}$ is much larger when multiple SMBHs are present. Values of $M_{\rm def}/M_{\rm bh} \approx 5$ have been observed in large elliptical galaxies (Graham 2004; Ferrarese et al. 2006; Hopkins & Hernquist 2010). Our model explains the occurrence of such systems. Since the star-star relaxation time in large elliptical galaxies in expected to be $\sim 10^{10}$ yr, we can expect them to carry the signature of core formation at high redshift due to multiple SMBHs. At lower redshift our simulation are applicable to spiral bulges, which have much lower relaxation time scale ($\sim 10^9$ yr). Indeed in the runs where a single black hole is left for $z \lesssim 2$, we find the formation of a Bahcall-Wolf cusp. This is consistent with the observed structure of the Milky Way bulge.

The above considerations regarding cores in galaxy luminosity profile are also applicable to dark matter cores. The ejection of dark matter particles by the black holes will produce a core similar in size to the stellar core.

7 OBSERVATIONAL SIGNATURES

From the results of our simulations described above, we expect about 30% of the galaxies within haloes with a present-day mass of $M_0 \approx 10^{14}$ M$_\odot$ to contain more than two SMBHs at redshifts $2 \lesssim z \lesssim 6$. For more massive haloes with $M_0 \gtrsim 10^{15}$ M$_\odot$, this fraction is almost 60%. However, since few such systems have been unambiguously observed so far, we consider some observational signatures that would indicate their existence[3]. Apart from their effect on the stellar mass distribution, multiple SMBH systems lead to an enhanced rate of tidal disruption of stars, modified gravitational wave signals compared to isolated BH binaries, and slingshot ejection of SMBHs from galaxies at high speeds.

From the results of scattering experiments, Chen et al. (2009) found that the stellar tidal disruption rates due to three-body interactions between a hard, unequal-mass SMBH binary with fixed separation and a bound stellar cusp is higher by several orders of magnitude than the corresponding rates for a single SMBH. In particular, they find that the stellar tidal disruption rate is about 1 yr^{-1} for an isothermal stellar cusp with $\sigma = 100$ km s^{-1} containing an SMBH binary of total mass 10^7 M$_\odot$. In comparison, the corresponding rate for a single 10^7 M$_\odot$ black hole is about 10^{-4} yr^{-1}. The duration of the tidal disruption phase is about 10^5 yr. This enhancement in the tidal disruption is due to the Kozai-Lidov effect and due to chaotic resonant scattering (Chen et al. 2011). Tidal disruption of a star results in about half of the stellar mass being inserted in bound elliptical orbits. When it falls back in the black hole, this mass gives rise to a bright UV/X-ray emission ("tidal flare") lasting for a few years. One such event may have already been recently observed in the form of high-energy transients that can be modeled as sudden accretion events onto an SMBH (Levan et al. 2011; Bloom et al. 2011; Zauderer et al. 2011).

We expect similar enhancement in the rate of stellar tidal disruption in systems with multiple black holes. Firstly, the presence of multiple SMBHs increases the combined tidal disruption cross section of the black holes. (Although this will only enhance the tidal disruption rate by a factor of a few.) Secondly, even before they closely interact, the presence of a third SMBH affects the tidal disruption event rate onto an SMBH binary by scattering stars into the binary's loss cone at a rate that increases as inverse square of its separation from the binary (Hoffman & Loeb 2007). Thirdly, as we saw above, multiple SMBH systems are likely to contain recoiled black holes, which have been kicked either due to anisotropic gravitational wave emission after coalescence, or due to the gravitational slingshot. Sudden recoil promptly fills the loss cone of these black holes. The resultant enhancement in the tidal disruption event rate can be substantial, increasing it up to 0.1 yr^{-1} (Stone & Loeb 2011). Furthermore, if their recoil velocity is not too high, these recoiled SMBHs oscillate around the stellar core with decreasing amplitude due to dynamical friction. This motion results in their repeated passages through the stellar core, thereby increasing the stellar tidal disruption event rate.

Another observational signature of systems with multiple SMBHs is gravitational waves (GWs). The GW emission from binary and triple SMBHs has been studied in the literature (Wyithe & Loeb 2003a; Sesana et al. 2004; Amaro-Seoane et al. 2010). Space-based detectors like the Laser Interferometer Space Antenna (LISA) are expected to be sensitive in the frequency range $\sim 10^{-4}$–10^{-1} Hz. This corresponds to the inspiral of SMBH systems with total mass $\sim 10^4 - 10^{10}$ M$_\odot$. Pulsar timing arrays (PTAs) like the Parkes PTA (Manchester 2008) and the European PTA (Janssen et al. 2008) and ground-based detectors like the North American Nanohertz Observatory for Gravitational Waves (Jenet et al. 2009) are sensitive to even lower frequencies of $\sim 10^{-8}$–10^{-6} Hz.

Yunes et al. (2011) studied modifications due to the presence

[3] Some systems with triple active galactic nuclei (AGNs) were reported so far. Examples are NGC 6166 and 7720 (Tonry 1984) and SDSSJ1027+1749 (Liu et al. 2011). The first two objects are cD galaxies at $z \approx 0.03$ and the latter is at $z \approx 0.06$. All three are kpc-scale triples. It is possible that NGC 6166 is simply a superposition of a central cD galaxy and two low-luminosity elliptical galaxies (Lauer et al. 1998).

of a secondary SMBH in the waveform of an extreme mass-ratio inspiral (EMRI) of a stellar mass objects into an SMBH. They find that a 10^6 $M_\odot$ SMBH will produce detectable modifications if it is within a few tenths of a parsec from the EMRI system, although this distance increases for higher mass SMBHs. In this paper, we have quantified the presence of such 'massive perturbers.' The resultant modifications to gravitational waveforms will be a distinct signature of multiple-SMBH systems. Futhermore, such systems often contain binaries that have phases of very high eccentricities, created via mechanisms like the Kozai-Lidov effect (Hoffman & Loeb 2007). Such binaries are expected to to emit intense bursts of high-frequency gravitational waves at the orbital periapsis (Amaro-Seoane et al. 2010). As a result, sources that would normally emit outside of the frequency windows of planned gravitational wave searches may be shifted into observable range. For example, Amaro-Seoane et al. (2010) find that a few to a hundred gravitational wave bursts could be produced at a detectable (1 ns) level within the PTA frequency range if the fraction of SMBH triplets is $\geqslant 0.1$.

Presence of triple SMBHs also has important implications for gravitational wave searches using matched-filtering by possibly requiring additional waveform templates (Amaro-Seoane & Freitag 2011).

Lastly, an observable signature of these systems will be the presence of wandering SMBHs in the large haloes (Hoffman & Loeb 2007). We have shown that about 10% of the SMBHs are ejected at velocities > 2000 km s $^{-1}$ due to the slingshot mechanism. This high-speed black holes will spend $1-10$ Gyr in the outskirts of the halo. However, it is not clear whether detecting this population of wandering black holes will be possible.

8 CONCLUSIONS

In this work, we have addressed the formation of galactic nuclei with mutiple SMBHs. We performed accurate N-body simulations of mergers of galactic nuclei with SMBHs in a cosmological setting. Our calculation uniquely incorporated cosmological mergers of galaxies with an accurate treatment of dynamical interactions between SMBHs and stars, which we achieved using the direct summation N-body code, NBODY6. The need for such simulations has been recognized in the literature (Merritt & Milosavljević 2005). Our main conclusions are as follows:

- In the absence of gas, high mass galaxies ($M_0 \gtrsim 10^{14}$ $M_\odot$ at $z = 0$) are generically expected to have had multiple SMBHs in their nuclei during their assembly history. Our simulations suggest that $\sim 30\%$ galaxies within haloes with a present-day mass of $M_0 \approx 10^{14}$ $M_\odot$ ($M_{z=6} \approx 10^{11}$ $M_\odot$) contain more than two SMBHs at redshifts $2 \lesssim z \lesssim 6$. For more massive haloes, with $M_0 \gtrsim 10^{15}$ $M_\odot$ ($M_{z=6} \approx 10^{12}$ $M_\odot$), this fraction is almost 60%. This is in contrast to lower-mass galaxies ($M_0 \approx 10^{12}$ $M_\odot$; $M_{z=6} \approx 10^{10}$ $M_\odot$), which rarely host more than two SMBHs in their nuclei at any moment in their assembly history.
- High mass galaxies as well as their low mass counterparts are rarely expected to retain more than two SMBHs in their nuclei at the present epoch. SMBH coalescence and ejection reduces the number of SMBHs on the time scale of a Gyr. Furthermore, major mergers are rare at lower redshift. We also find that the number of SMBHs in galactic nuclei is rarely reduced to zero at $z = 0$. Less than 5% of our high-mass runs resulted in such galaxies.
- SMBH coalescence is common at high redshifts. Subsequent recoil due to anisotropic gravitational wave emission often results in escaping SMBHs. Some of these SMBHs add to the wandering population of black holes in the galactic halo. In a few cases, this process also results in galactic nuclei with no SMBH near their centres. BH-BH interaction also leads to ejected SMBHs via the slingshot mechanism. While most of ejected SMBHs have velocities $\lesssim 500$ km s^{-1}, about 10% SMBHs are ejected at very high velocities exceeding 2000 km s^{-1}. We also find binary SMBH ejection in $\lesssim 10\%$ of the cases.
- Multiple SMBHs have a strong effect on the stellar distribution due to three-body interactions and core passages. The resulting mass deficit is usually much larger than that due to a single SMBH binary because of resonant BH-BH interactions and GW recoil of the BH remnant. We observe long-term oscillations of the BH-core system that could explain observations of offset AGNs. This has implications for recent observations by Civano et al. (2010) of a $z = 0.359$ system that potentially contains a recoiled BH.
- The presence of multiple SMBHs will have important effects on the rate of tidal disruption of stars in galactic nuclei due to enhanced tidal disruption cross section, scattering of stars by other BHs, prompt loss cone refilling due to GW recoil and gravitational slingshot. Similarly, the presence of more than two BHs in a hierarchical triple is expected to leave a signature in the GW emission from the inner binary. This signature could be observed with future GW observatories, such as LISA. Finally, we also expect such systems to give rise to a distinct population of wandering SMBHs that could travel in large haloes over long time scales of a few Gyrs.

The presence of gas could alter the above picture to some extent. However, simulations of binary BHs in gaseous environment have not reached sufficient resolution to confirm this. Moreover, we expect that at high redshifts, AGN activity triggered by galaxy mergers could efficiently drive gas away from the shallow potential wells of the galaxy. Our work can also be extended by calculating late stages of binary SMBH evolution more consistently. New regularization techniques to do this are now available (Aarseth 2003); we defer their use to future work. Furthermore, multiple SMBH systems can also form in additional ways, for example by fragmentation of disks (Goodman & Tan 2004). However, these systems would evolve by migration (Kocsis et al. 2011) on a much shorter time scale than considered here.

ACKNOWLEDGEMENTS

We acknowledge advice on various aspects of our simulations from Sverre Aarseth and would like to thank him for making his codes available. GK also acknowledges discussion with Jasjeet S. Bagla, Hagai Perets and Yue Shen, and the Institute for Theory and Computation for hospitality. Our simulations were run on the Odyssey cluster supported by the FAS Sciences Division Research Computing Group at Harvard University. The Millennium Simulation databases used in this paper and the web application providing online access to them were constructed as part of the activities of the German Astrophysical Virtual Observatory. This research was supported in part by a Fulbright-Nehru Professional and Predoctoral Fellowship from the US-India Educational Foundation, by NSF grant AST-0907890 and NASA grants NNX08AL43G and NNA09DB30A.

REFERENCES

Aarseth S. J., 1999, PASP, 111, 1333

Aarseth S. J., 2003, Gravitational N-Body Simulations
Ahmad A., Cohen L., 1973, Journal of Computational Physics, 12, 389
Amaro-Seoane P., Freitag M. D., 2011, MNRAS, 412, 551
Amaro-Seoane P., Sesana A., Hoffman L., Benacquista M., Eichhorn C., Makino J., Spurzem R., 2010, MNRAS, 402, 2308
Armitage P. J., Natarajan P., 2002, ApJ, 567, L9
Baker J. G., Centrella J., Choi D.-I., Koppitz M., van Meter J., 2006, Physical Review Letters, 96, 111102
Baker J. G., Centrella J., Choi D.-I., Koppitz M., van Meter J. R., Miller M. C., 2006, ApJ, 653, L93
Barkana R., Loeb A., 2001, Phys. Rep., 349, 125
Begelman M. C., Blandford R. D., Rees M. J., 1980, Nature, 287, 307
Bekenstein J. D., 1973, ApJ, 183, 657
Benson A. J., 2005, MNRAS, 358, 551
Berczik P., Merritt D., Spurzem R., Bischof H.-P., 2006, ApJ, 642, L21
Binney J., Tremaine S., 2008, Galactic Dynamics: Second Edition. Princeton University Press
Blaes O., Lee M. H., Socrates A., 2002, ApJ, 578, 775
Blecha L., Cox T. J., Loeb A., Hernquist L., 2011, MNRAS, 412, 2154
Bloom J. S., Giannios D., Metzger B. D., Cenko S. B., Perley D. A., Butler N. R., Tanvir N. R., Levan A. J., O' Brien P. T., Strubbe L. E., De Colle F., Ramirez-Ruiz E., Lee W. H., Nayakshin S., Quataert E., et al., 2011, ArXiv e-prints
Bogdanović T., Reynolds C. S., Miller M. C., 2007, ApJ, 661, L147
Boylan-Kolchin M., Ma C., Quataert E., 2008, MNRAS, 383, 93
Boylan-Kolchin M., Springel V., White S. D. M., Jenkins A., Lemson G., 2009, MNRAS, 398, 1150
Bromm V., Loeb A., 2003, ApJ, 596, 34
Bundy K., Treu T., Ellis R. S., 2007, ApJ, 665, L5
Campanelli M., Lousto C., Zlochower Y., Merritt D., 2007a, ApJ, 659, L5
Campanelli M., Lousto C. O., Zlochower Y., Merritt D., 2007b, Physical Review Letters, 98, 231102
Chandrasekhar S., 1943, ApJ, 97, 255
Chatterjee P., Hernquist L., Loeb A., 2002, ApJ, 572, 371
Chen X., Madau P., Sesana A., Liu F. K., 2009, ApJ, 697, L149
Chen X., Sesana A., Madau P., Liu F. K., 2011, ApJ, 729, 13
Civano F., Elvis M., Lanzuisi G., Jahnke K., Zamorani G., Blecha L., Bongiorno A., Brusa M., Comastri A., Hao H., Leauthaud A., Loeb A., Mainieri V., Piconcelli E., Salvato M., Scoville N., Trump J., Vignali C., et al., 2010, ApJ, 717, 209
Colpi M., Dotti M., 2009, ArXiv e-prints
Colpi M., Mayer L., Governato F., 1999, ApJ, 525, 720
Eisenstein D. J., Loeb A., 1995, ApJ, 443, 11
Escala A., Larson R. B., Coppi P. S., Mardones D., 2004, ApJ, 607, 765
Escala A., Larson R. B., Coppi P. S., Mardones D., 2005, ApJ, 630, 152
Faber S. M., Tremaine S., Ajhar E. A., Byun Y.-I., Dressler A., Gebhardt K., Grillmair C., Kormendy J., Lauer T. R., Richstone D., 1997, AJ, 114, 1771
Fakhouri O., Ma C., Boylan-Kolchin M., 2010, MNRAS, 406, 2267
Fan X., Narayanan V. K., Lupton R. H., Strauss M. A., Knapp G. R., Becker R. H., et al., 2001, AJ, 122, 2833
Ferrarese L., 2002, ApJ, 578, 90
Ferrarese L., Côté P., Jordán A., Peng E. W., Blakeslee J. P., Piatek S., Mei S., Merritt D., Milosavljević M., Tonry J. L., West M. J., 2006, ApJS, 164, 334
Ferrarese L., Ford H., 2005, Space Sci. Rev., 116, 523
Ferrarese L., Merritt D., 2000, ApJ, 539, L9
Freitag M., Amaro-Seoane P., Kalogera V., 2006, ApJ, 649, 91
Gebhardt K., Bender R., Bower G., Dressler A., Faber S. M., Filippenko A. V., Green R., Grillmair C., Ho L. C., Kormendy J., Lauer T. R., Magorrian J., Pinkney J., Richstone D., Tremaine S., 2000, ApJ, 539, L13
Genzel R., Schödel R., Ott T., Eisenhauer F., Hofmann R., Lehnert M., Eckart A., Alexander T., Sternberg A., Lenzen R., Clénet Y., Lacombe F., Rouan D., Renzini A., Tacconi-Garman L. E., 2003, ApJ, 594, 812
Gnedin O. Y., 2003, ApJ, 589, 752
González J. A., Hannam M., Sperhake U., Brügmann B., Husa S., 2007, Physical Review Letters, 98, 231101
Goodman J., Tan J. C., 2004, ApJ, 608, 108
Graham A. W., 2004, ApJ, 613, L33
Gualandris A., Merritt D., 2008, ApJ, 678, 780
Gültekin K., Richstone D. O., Gebhardt K., Lauer T. R., Tremaine S., Aller M. C., Bender R., Dressler A., Faber S. M., Filippenko A. V., Green R., Ho L. C., Kormendy J., Magorrian J., Pinkney J., Siopis C., 2009, ApJ, 698, 198
Haehnelt M. G., Kauffmann G., 2002, MNRAS, 336, L61
Haiman Z., Loeb A., 1999, ApJ, 521, L9
Heggie D. C., Mathieu R. D., 1986, in P. Hut & S. L. W. McMillan ed., The Use of Supercomputers in Stellar Dynamics Vol. 267 of Lecture Notes in Physics, Berlin Springer Verlag, Standardised Units and Time Scales. pp 233–+
Heinämäki P., 2001, A&A, 371, 795
Herrmann F., Hinder I., Shoemaker D., Laguna P., 2007, Classical and Quantum Gravity, 24, 33
Hoffman L., Loeb A., 2007, MNRAS, 377, 957
Hopkins P. F., Hernquist L., 2010, MNRAS, 407, 447
Hopkins P. F., Hernquist L., Cox T. J., Di Matteo T., Robertson B., Springel V., 2006, ApJS, 163, 1
Hopkins P. F., Hernquist L., Cox T. J., Robertson B., Krause E., 2007, ApJ, 669, 45
Hut P., Rees M. J., 1992, MNRAS, 259, 27P
Iwasawa M., Funato Y., Makino J., 2006, ApJ, 651, 1059
Janssen G. H., Stappers B. W., Kramer M., Purver M., Jessner A., Cognard I., 2008, in C. Bassa, Z. Wang, A. Cumming, & V. M. Kaspi ed., 40 Years of Pulsars: Millisecond Pulsars, Magnetars and More Vol. 983 of American Institute of Physics Conference Series, European Pulsar Timing Array. pp 633–635
Jenet F., Finn L. S., Lazio J., Lommen A., McLaughlin M., Stairs I., Stinebring D., Verbiest J., Archibald A., Arzoumanian Z., Backer D., Cordes J., Demorest P., Ferdman R., Freire P., other 2009, ArXiv e-prints
Jiang C. Y., Jing Y. P., Faltenbacher A., Lin W. P., Li C., 2008, ApJ, 675, 1095
Kauffmann G., Haehnelt M., 2000, MNRAS, 311, 576
Khan F., Just A., Merritt D., 2011, ArXiv e-prints
Khochfar S., Burkert A., 2006, A&A, 445, 403
Kocsis B., Yunes N., Loeb A., 2011, ArXiv e-prints
Kulkarni S. R., Hut P., McMillan S., 1993, Nature, 364, 421
Lacey C., Cole S., 1993, MNRAS, 262, 627
Lauer T. R., Faber S. M., Ajhar E. A., Grillmair C. J., Scowen P. A., 1998, AJ, 116, 2263
Levan A. J., Tanvir N. R., Cenko S. B., Perley D. A., Wiersema K., Bloom J. S., Fruchter A. S., de Ugarte Postigo A., O'Brien P. T., Butler N., van der Horst A. J., Leloudas G., Morgan A. N.,

Misra K., Bower G., Farihi J., et al., 2011, ArXiv e-prints
Li Y., Hernquist L., Robertson B., Cox T. J., Hopkins P. F., Springel V., Gao L., Di Matteo T., Zentner A. R., Jenkins A., Yoshida N., 2007, ApJ, 665, 187
Liu X., Shen Y., Strauss M. A., 2011, ArXiv e-prints
Loeb A., 2010, Phys. Rev. D, 81, 047503
Loeb A., Rasio F. A., 1994, ApJ, 432, 52
Lousto C. O., Zlochower Y., 2009, Phys. Rev. D, 79, 064018
Magorrian J., Tremaine S., Richstone D., Bender R., Bower G., Dressler A., Faber S. M., Gebhardt K., Green R., Grillmair C., Kormendy J., Lauer T., 1998, AJ, 115, 2285
Makino J., 1997, ApJ, 478, 58
Makino J., Aarseth S. J., 1992, PASJ, 44, 141
Makino J., Ebisuzaki T., 1996, ApJ, 465, 527
Makino J., Funato Y., 2004, ApJ, 602, 93
Manchester R. N., 2008, in C. Bassa, Z. Wang, A. Cumming, & V. M. Kaspi ed., 40 Years of Pulsars: Millisecond Pulsars, Magnetars and More Vol. 983 of American Institute of Physics Conference Series, The Parkes Pulsar Timing Array Project. pp 584–592
Marconi A., Hunt L. K., 2003, ApJ, 589, L21
McLure R. J., Dunlop J. S., 2002, MNRAS, 331, 795
Menou K., Haiman Z., Narayanan V. K., 2001, ApJ, 558, 535
Merritt D., 2000, in F. Combes, G. A. Mamon, & V. Charmandaris ed., Dynamics of Galaxies: from the Early Universe to the Present Vol. 197 of Astronomical Society of the Pacific Conference Series, Black Holes and Galaxy Evolution. pp 221–+
Merritt D., 2006, ApJ, 648, 976
Merritt D., Mikkola S., Szell A., 2007, ApJ, 671, 53
Merritt D., Milosavljević M., 2005, Living Reviews in Relativity, 8, 8
Merritt D., Poon M. Y., 2004, ApJ, 606, 788
Merritt D., Szell A., 2006, ApJ, 648, 890
Mikkola S., Aarseth S. J., 1990, Celestial Mechanics and Dynamical Astronomy, 47, 375
Mikkola S., Valtonen M. J., 1990, ApJ, 348, 412
Milosavljević M., Merritt D., 2001, ApJ, 563, 34
Milosavljević M., Merritt D., 2003a, ApJ, 596, 860
Milosavljević M., Merritt D., 2003b, in J. M. Centrella ed., The Astrophysics of Gravitational Wave Sources Vol. 686 of American Institute of Physics Conference Series, The Final Parsec Problem. pp 201–210
Miralda-Escudé J., Gould A., 2000, ApJ, 545, 847
Monaco P., Fontanot F., Taffoni G., 2007, MNRAS, 375, 1189
Mortlock D. J., Warren S. J., Venemans B. P., Patel M., Hewett P. C., McMahon R. G., Simpson C., Theuns T., Gonzáles-Solares E. A., Adamson A., Dye S., Hambly N. C., Hirst P., Irwin M. J., Kuiper E., Lawrence A., Röttgering H. J. A., 2011, Nature, 474, 616
Peng C. Y., Impey C. D., Ho L. C., Barton E. J., Rix H.-W., 2006, ApJ, 640, 114
Peres A., 1962, Physical Review, 128, 2471
Peters P. C., 1964, Phys. Rev., 136, 1224
Pretorius F., 2005, Physical Review Letters, 95, 121101
Quinlan G. D., 1996, New Astron., 1, 35
Quinlan G. D., Hernquist L., 1997, New Astron., 2, 533
Richstone D., Ajhar E. A., Bender R., Bower G., Dressler A., Faber S. M., Filippenko A. V., Gebhardt K., Green R., Ho L. C., Kormendy J., Lauer T. R., Magorrian J., Tremaine S., 1998, Nature, 395, A14+
Saslaw W. C., Valtonen M. J., Aarseth S. J., 1974, ApJ, 190, 253
Sesana A., Haardt F., Madau P., Volonteri M., 2004, ApJ, 611, 623
Shen Y., 2009, ApJ, 704, 89
Sheth R. K., Tormen G., 1999, MNRAS, 308, 119
Sigurdsson S., Hernquist L., 1993, Nature, 364, 423
Sijacki D., Springel V., Di Matteo T., Hernquist L., 2007, MNRAS, 380, 877
Springel V., White S. D. M., Jenkins A., Frenk C. S., Yoshida N., Gao L., Navarro J., Thacker R., Croton D., Helly J., Peacock J. A., Cole S., Thomas P., Couchman H., Evrard A., Colberg J., Pearce F., 2005, Nature, 435, 629
Stone N., Loeb A., 2011, MNRAS, 412, 75
Taffoni G., Mayer L., Colpi M., Governato F., 2003, MNRAS, 341, 434
Tanaka T., Haiman Z., 2009, ApJ, 696, 1798
Taylor J. E., Babul A., 2001, ApJ, 559, 716
Tonry J. L., 1984, ApJ, 279, 13
Tremaine S., Gebhardt K., Bender R., Bower G., Dressler A., Faber S. M., Filippenko A. V., Green R., Grillmair C., Ho L. C., Kormendy J., Lauer T. R., Magorrian J., Pinkney J., Richstone D., 2002, ApJ, 574, 740
Valtonen M. J., 1976, A&A, 46, 435
Valtonen M. J., Mikkola S., Heinamaki P., Valtonen H., 1994, ApJS, 95, 69
van den Bosch F. C., Lewis G. F., Lake G., Stadel J., 1999, ApJ, 515, 50
Volonteri M., 2007, ApJ, 663, L5
Volonteri M., Haardt F., Madau P., 2003, ApJ, 582, 559
Volonteri M., Rees M. J., 2006, ApJ, 650, 669
Wetzel A. R., Cohn J. D., White M., 2009, MNRAS, 395, 1376
Wyithe J. S. B., Loeb A., 2003a, ApJ, 590, 691
Wyithe J. S. B., Loeb A., 2003b, ApJ, 595, 614
Xu G., Ostriker J. P., 1994, ApJ, 437, 184
Yoo J., Miralda-Escudé J., 2004, ApJ, 614, L25
Yu Q., 2002, MNRAS, 331, 935
Yunes N., Coleman Miller M., Thornburg J., 2011, Phys. Rev. D, 83, 044030
Zauderer B. A., Berger E., Soderberg A. M., Loeb A., Narayan R., Frail D. A., Petitpas G. R., Brunthaler A., Chornock R., Carpenter J. M., Pooley G. G., Mooley K., Kulkarni S. R., et al., 2011, ArXiv e-prints
Zentner A. R., Berlind A. A., Bullock J. S., Kravtsov A. V., Wechsler R. H., 2005, ApJ, 624, 505